M.F. van Dommele

Towards more continuous feedback on soft tissue anatomy during percutaneous needle placement in the liver

Exploring the use of endovascular markers to track the tumor location

Delft University of Technology

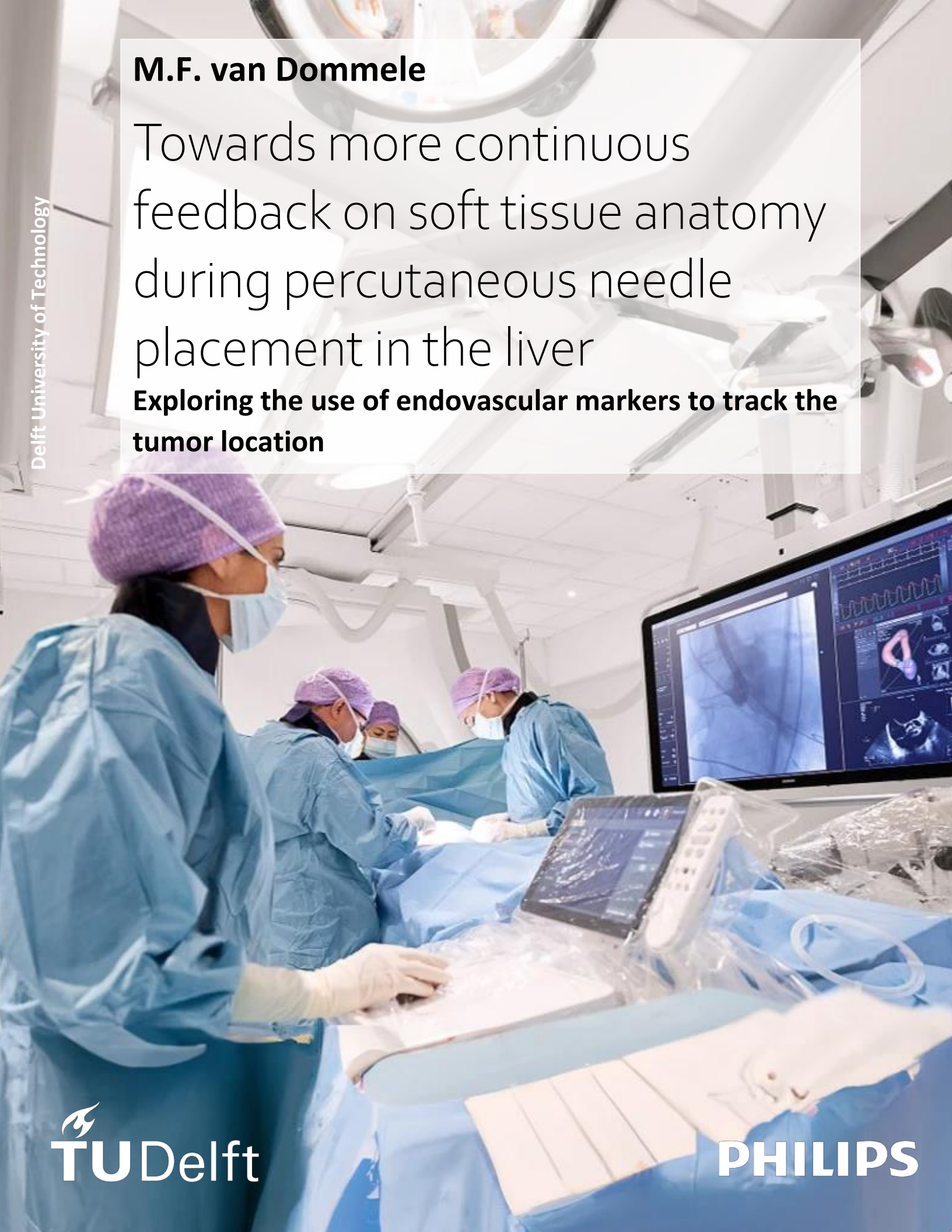

TU Delft

PHILIPS

MSc Thesis

Towards more continuous feedback on soft tissue anatomy during percutaneous needle placement in the liver

by

M.F. van Dommele

Student Name	Student Number
M.F. van Dommele	4470877

Supervisor TU Delft:	dr. D. Dodou
Supervisor Philips:	P. Goossen-Nachtigall, dr. A. Muris
Institution:	Delft University of Technology
Place:	Faculty of Mechanical, Maritime and Materials Engineering, Delft
Project Duration:	February, 2022 - January, 2023

Cover Image: The Philips Azurion next generation image-guided therapy platform (internal media library Philips)

TU Delft

PHILIPS

Preface

I am proud to introduce to you my final master's thesis, which focuses on soft-tissue deformation and tracking in percutaneous needle procedures in the liver. The project was conducted in collaboration between the Biomedical Engineering department at the Delft University of Technology and the research department of Image-Guided Therapy Systems at Philips Healthcare in Best, the Netherlands. The Vrije Universiteit medical center (VUmc) was also involved in conducting the experiments.

I would like to express my gratitude to all the people who helped me during my project. First, I would like to thank my supervisor, Dr. D. Dodou for the support during the graduation process and the clarifying feedback. Your expertise ensured a new perspective and provided a pleasant and critical view. Thank you so much for the weekly meetings and the support in the past year!

Second, I would like to thank P. Goossen-Nachtigall and Dr. A.H. Muris from Philips. Thank you for daring to take up the challenge with me and for accepting me on this exploratory research project. I want to thank you both for your warm welcome to Best and your commitment to my thesis, even if that meant staying in Best until 22.30. It has been a valuable learning journey to work alongside you both and benefit from your insights and experience. I could not have done this without you and I really enjoyed my time in Best with you both professionally and personally.

Third, I also want to thank Prof. Dr. Meijerink, S. van der Lei and the interventional radiology research department from the VUmc. Your team helped me tremendously with the experiment setup. Thank you for your creativity and flexibility during our collaboration.

Fourth, I want to express my gratitude to all the other people that were involved in shaping or brainstorming my thesis: Rogier van der Wacht, William van der Sterren, Marco Verstege, Kajo van der Marel, Rens Schoones, Peter van de Haar, Yno Prevoo, Marlein Vogels, prof. Dr. De Winter, and everybody else who was up for a quick coffee chat or brainstorm about percutaneous needle procedures.

Finally, I would like to thank my family and friends for their support, motivation, and inspiration during my graduation project.

Enjoy reading!

M.F. van Dommele
Delft, January 2023

Contents

1

Paper

Towards continuous feedback on soft tissue anatomy during a percutaneous needle procedure in the liver by tracking endovascular markers

M.F. van Dommele, Master Thesis Biomedical Engineering
Faculty of 3mE, Technical University Delft, The Netherlands
Department of Clinical Science, Philips Image Guided Therapy Systems, Best, The Netherlands

***Abstract* – Percutaneous needle procedures (PNPs) are minimally invasive procedures that use imaging guidance to diagnose or treat medical conditions. In the treatment of liver cancer, PNPs are becoming increasingly used due to their shorter recovery times and lower complication rates. However, needle placement during PNPs can be challenging due to a lack of direct visualization of the target and liver tissue deformation caused by respiratory motion, patient (re)positioning, and needle insertion. Currently, no imaging modality provides continuous, qualitative visualization while maintaining acceptable radiation levels. Continuous feedback during PNPs could improve needle placement accuracy by enabling real-time adjustments in response to tissue deformation. Previous studies have used external- and internal markers for continuous feedback, but these markers have not been able to fully capture tumor displacement and the underlying causes of deformation. Endovascular insertion is a potential solution to this problem - it involves placing the marker close to the tumor by inserting it through the blood vessels. Here, we present exploratory research that aims to investigate the possibility of using an endovascular marker to capture the displacement of a liver tumor during a PNP.**

An ex-vivo porcine liver with artificially created tumors and endovascular catheter markers was used. In the first experiment, robotic-assisted needle insertion was performed on seven tumors with a 13-gauge ablation needle. The second experiment involved simulating respiratory motion with an inflatable sachet to mimic the lungs and create a representable blow zone (the area affected by the inflated sachet). The displacement of the tumor- and endovascular catheter markers were tracked in the x-, y-, and z-directions using a C-arm system making Cone Beam Computed Tomography (CBCT). The x- and y-directions represents the horizontal plane within the liver, and the z-direction is the vertical plane (the direction of the ablation needle). The average offset in millimeters was calculated to quantify the error between the tumor- and catheter marker displacement.

The results of needle insertion showed that catheter markers placed 8-28 mm from the tumor could deduce tumor displacement in the x-direction, with a maximum offset of 1.23 mm. The catheter markers placed 8-13 mm from the tumor were also able to deduce displacement in the z-direction with a maximum offset of 0.23 mm and in Euclidean distance (total path length as measured using Pythagoras' theorem) with a maximum offset of 0.73 mm. Furthermore, the results indicated that, on average, catheter markers placed 8-28 mm from the tumor were able to accurately deduce tumor displacement for needle insertion depths of 0-15 mm. During respiratory motion simulation, tumor- and catheter marker displacement was influenced more by blow zone location than the distance between them. To apply these findings to the human body, it is recommended that the endovascular marker will be positioned in the same sagittal (longitudinal) and coronal (frontal) plane as the tumor. In this study, catheter markers could be used to deduce tumor displacement for inflation volumes of 0-500 ml, which is the typical resting breathing volume.

In conclusion, this study demonstrated that the ability to use endovascular catheter markers to deduce tumor displacement during a percutaneous needle procedure is influenced by the distance between the tumor- and the catheter marker, the depth of the needle, the inflation volume of simulated lungs, and whether the marker is positioned in the same sagittal and coronal plane in relation to the tumor. Future research should focus on determining the optimal number and location of endovascular markers, including a bigger variation and spread of tumor locations, and adjusting insertion techniques, to further realize the clinical applicability of endovascular catheter markers in percutaneous needle procedures.

***Keywords* – Ex-vivo study, Internal markers, Liver, Needle procedure, Percutaneous therapy, Soft-tissue motion, Tumor tracking**

Nomenclature

C	Catheter
CBCT	Cone Beam Computed Tomography
CT	Computed Tomography
FM	Fiducial Marker
MRI	Magnetic Resonance Imaging
PNP	Percutaneous Needle Procedure
T	Tumor
US	Ultrasound

I. INTRODUCTION

Over the last few decades, the use of minimally invasive techniques in interventional oncology has led to a revolution in cancer treatment. Minimally invasive techniques involve the use of small incisions and specialized instruments to access a specific area inside the patient. This approach contrasts with traditional open surgery, which involves large incisions to expose the target area inside the body. Minimally invasive techniques have many advantages over open surgery, including reduced trauma to the body, shorter recovery times, and a lower complication rate [1]. However, unlike in open surgery, the interventional oncologist does not have a direct visual view of the internal anatomy of the patient during minimally invasive procedures but depends on imaging technology and guidance. In liver cancer treatment, minimally invasive techniques have become increasingly used due to the aforementioned advantages [2]. One of the most common minimally invasive procedures for the liver is a percutaneous needle procedure (PNP). A PNP involves the insertion of a needle through the skin to target a tumor inside the patient. Within the field of interventional oncology, PNPs serve both diagnostic (e.g. biopsies to identify tissue) and

therapeutic (e.g. tumor ablation) purposes. Even though the intended purposes may differ, both diagnostic and therapeutic procedures require accurate needle placement [3]. Thus, the accuracy of tracking the target and using the knowledge about the real-time anatomy to plan the needle trajectory is vital for the success of the procedures. Misplacement of the needle might lead to damaging healthy tissue, false diagnosis, and prolonged procedure time [4, 5, 6].

Intraoperative guidance is needed to support the interventional oncologist in needle placement; mainly Ultrasound (US), Computed Tomography (CT), a C-arm system (e.g. CT-fluoroscopy or Cone Beam Computed Tomography (CBCT)), and Magnetic Resonance Imaging (MRI) are used [7]. US and CT are the most used; US is the only modality that provides continuous and real-time imaging without ionizing radiation. However, it does not provide an accurate image of deep-seated tumors, is highly sensitive to artifacts and the quality of the acquired image and interpretation is dependent on the operator [8]. CT provides cross-sectional imaging in three dimensions, but does not provide continuous imaging, uses ionizing radiation, has low soft tissue contrast, and can make patient accessibility challenging due to the limited physical space created by the doughnut-shaped machine [7, 9]. No single modality is universally used; each modality has its benefits and drawbacks. The selection of an imaging modality for a PNP is influenced by the preferences and availability of the hospital and the interventional oncologist [10]. A challenge in intraoperative guidance is the soft tissue deformation in the region of interest. This deformation is caused by various movements, including respiratory motion, patient (re)positioning, and the movement induced by needle placement [11, 12]. Currently, there is no imaging technique that allows for continuous, high-quality visualization while maintaining acceptable levels of ionizing radiation exposure. As a result, interventional oncologists rely on previous scans and their own experience when performing procedures [9]. Therefore, finding a solution to the challenge of accurately targeting tumors is crucial for optimizing patient outcomes and improving the effectiveness of cancer treatment [13, 14].

Previous research in the field has identified several approaches for improving intraoperative guidance, including; the use of image processing to fuse multiple imaging modalities, the deployment of internal- or external fiducial markers (FMs) to track displacement, and the development of models or algorithms that can non-invasively predict displacement [15]. Of these approaches, the use of models is the most desirable due to their low invasiveness and automation, which eliminates user dependence. However, current models and algorithms rely on indirect signals and surrogates such as FM displacement on the abdomen or imaging to visualize diaphragm displacement, rather than considering all possible causes of deformation which is necessary for training future models [16, 17, 18, 19, 20, 21]. The reliance on surrogates can result in an incomplete understanding of tumor displacement, leading to potential inaccuracies in targeting [22]. To address this issue, FMs that are implanted near the target may be able to capture the "total displacement". It is considered to be the "total displacement" within a margin of error of 2.00 mm, based on a threshold currently used by physicians to assess a technique and the maximum degree of error used in Guiu et al. [23].

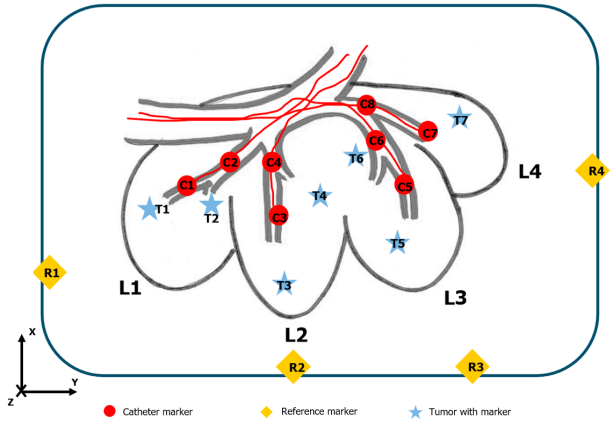

Figure 1: *Schematic drawing of porcine liver set-up in bucket. Four lobes (L1-L4), seven tumor sites (T1-T7), eight endovascular catheter markers (C1-C8), four reference markers (R1-R4) and the x-, y-, and z-directions.*

An implantable sensor, as used by Kok et al. [24], can be inserted near a target in the body as an internal marker. These sensors or markers can be inserted either percutaneous (through the skin) or endovascular (through the arteries). Currently, the main methods of using internal markers for targeting the liver include the percutaneous insertion of golden beads, or the use of other internal FMs [25, 26, 27]. Endovascular insertion, in which the blood vessels are used as a demarcated path, has the advantage of reaching deep liver targets without traversing multiple tissue layers. Therefore, we will investigate the potential use of endovascular markers for deducing tumor displacement, as they have the potential to provide more accurate displacement data compared to other internal fiducials due to their proximity to the target.

Previous research has primarily examined the deformation of soft tissue during PNP in relation to respiratory motion [18, 28, 29, 30, 31]. However, needle insertion itself also contributes to the deformation of the soft tissue during PNP [32]. This study will focus on the deformation caused by both respiratory motion and needle placement. While respiratory motion leads to larger deformation, it is more predictable, whereas needle placement results in smaller deformation but is less predictable.

The objective of this exploratory research is to evaluate the feasibility of using an endovascular marker to capture the displacement of a tumor in an ex-vivo porcine liver during a PNP. The study aims to answer the following questions: What is the relationship between the displacement of a tumor and an endovascular marker during needle insertion? What is the relationship between the displacement of a tumor and an endovascular marker during respiratory motion? What factors influence the relationship between a tumor and an endovascular marker during a PNP, and how do these factors affect the relationship? Additionally, the overarching research question is: How can an endovascular marker be used during a PNP in the liver to track and deduce the displacements of a tumor?

Figure 2: *Preparing the setup. F.l.t.r.: The top left picture shows the liver positioned on the latex gloves, in pink the endovascular catheters - the bottom picture shows the liver fixated with agar - the middle picture shows preparing the liver by inserting agar spheres - the right picture shows the robot arm before needle insertion. The black and white stickers on the liver are the markers for ClarifEye.*

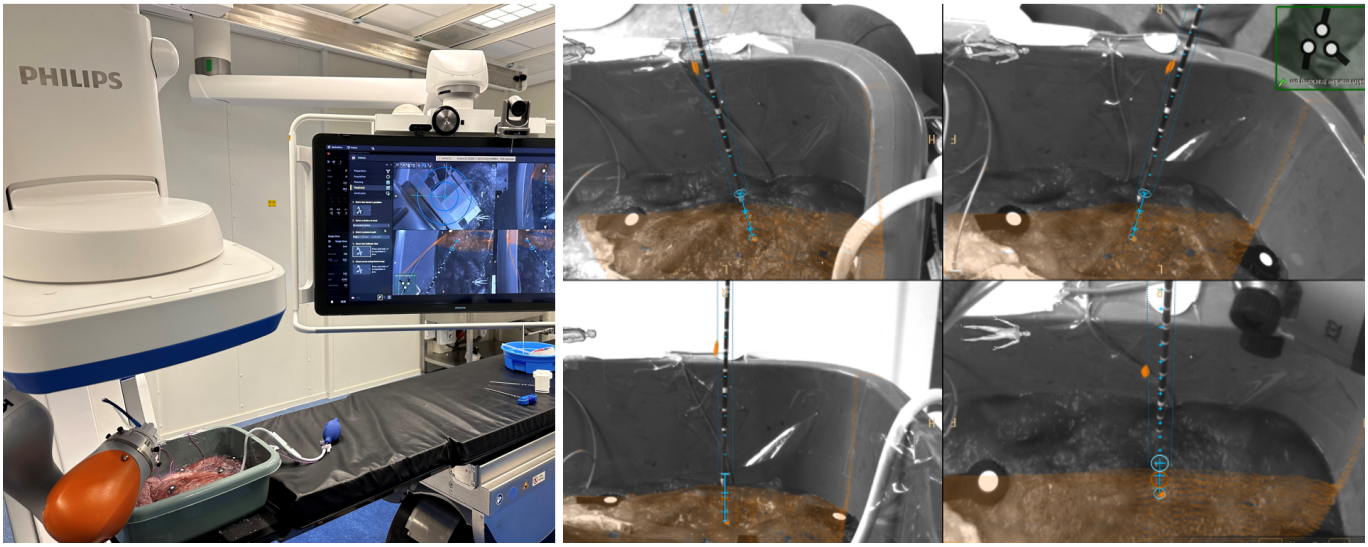

Figure 3: *Aligning the ablation needle with ClarifEye. F.l.t.r: The robot arm aligns with the bulls-eye view on the physical monitor. - The screen of ClarifEye with the planned needle projected in augmented reality from different perspectives. This allows for the appropriate positioning of the robot arm holding the 13-gauge ablation needle.*

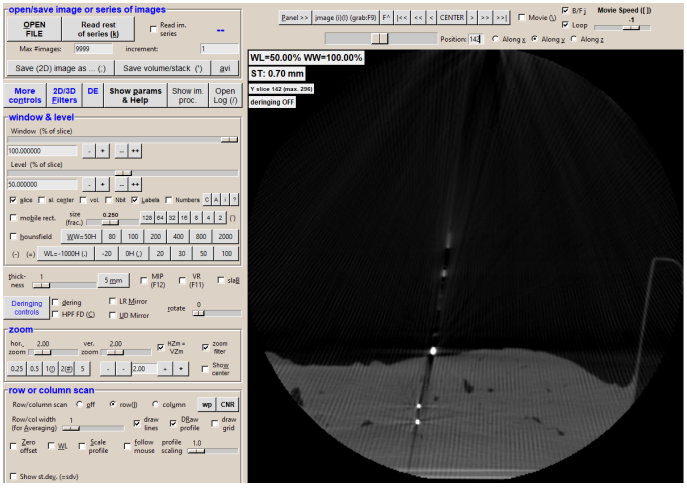

Figure 4: *Preview of the CBCT image for T6 in the image viewer dView. The needle is the white dot coming into the liver, the middle white dot is the tumor marker and the lower white dot is the endovascular catheter marker. The needle path can be deduced from the image by looking at the needle direction; the extension of the path is pointed toward the endovascular marker.*

II. MATERIALS AND METHODS

A. Study set-up with ex-vivo liver preparation

An ex-vivo porcine liver (weighing approximately 2.1 kg) was used in the experiment conducted on the 16th of November 2022 in a non-clinical lab at Philips Healthcare (Best, The Netherlands) to simulate robotic-assisted needle insertion and respiratory motion. A porcine liver is considered a suitable model for studying endovascular markers due to its similarity to the liver blood supply of a human [33].

Seven artificial tumors were created in the porcine liver (T1-T7 in Figure 1), by injecting agar sphere-like shapes using a syringe (BD Plastipak, Becton Dickinson, United States) and a 16-gauge tracked Jamshidi needle (ClarifEye Needle, Philips Healthcare, Best, The Netherlands). Agar was selected for its consistency and size to replicate the properties of a tumor. From the literature, it is known that the hardness of a tumor is significantly greater than that of normal liver tissue [34]. Three physicians confirmed the hardness of the agar by comparing it to normal liver tissue and classified it as having a density between normal and medium hard tissue on a hardness scale (2-3 on a hardness scale, see Appendix VII). The initial plan was to insert eight tumors, however, due to a mismeasurement, only seven tumors were taken into account in the experiment. The distance between the tumor- and the catheter marker was varied. The tumor-catheter pairs were categorized into three groups: group 1 with the catheter marker close to the tumor (min-max 8-13 mm), group 2 with the catheter marker medium far from the tumor (min-max 18-19 mm), and group 3 with the catheter marker far from the tumor (min-max 26-28 mm).

After injecting the agar, a metal fiducial marker (1.6 mm diameter) was placed at the center of each tumor to enable tracking during the experiment. Four endovascular catheters (Cragg-McNamara® Valved Infusion Catheter, Medtronic B.V., Ireland) were advanced, each with two radio-opaque markings serving as endovascular catheter markers (C1-C8, see Figure 1) visible on imaging. The catheters were advanced into the hepatic veins, advancing into the arteries was not feasible in this experimental setup. Four metal FMs (2 mm diameter) were attached to the inside of the plastic bucket as reference markers (R1-R4, see Figure 1) to recalibrate the data and exclude displacements unrelated to the experiment.

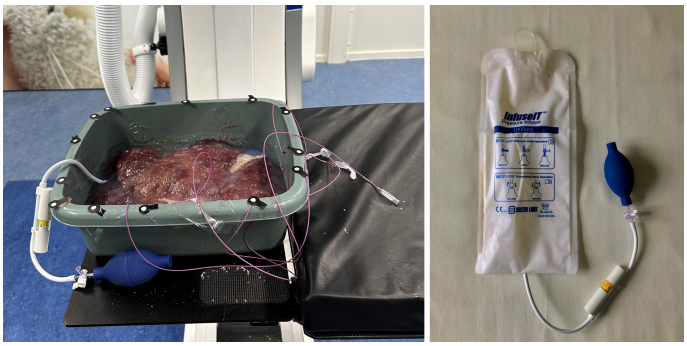

Figure 5: *The setup for the respiratory motion simulation experiment. The medical infusion pump sachet shown on the right is positioned underneath the liver.*

The liver was placed in a plastic bucket that contained six latex gloves filled with water on the bottom to simulate the intestines. Agar was used to fixate the liver on top of the gloves and to mimic the connective tissues that are surrounding the liver in the human body [35] (see Figure 2). The detailed protocol of liver preparation and agar fixation can be found in Appendix VII. The C-arm system (Azurion, Philips Healthcare, Best, The Netherlands) was selected for this experiment due to its ability to offer a flexible workspace and acquire 2D fluoroscopy and 3D CBCT images.

B. Experiment design

Two experiments were performed during this study. First, the effect of robotic-assisted needle insertion on the displacement of the tumor- and catheter markers was investigated. Second, the effect of simulated respiratory motion on the displacement of the tumor- and catheter markers was investigated (see Appendix VII.for detailed protocol).

1) Robotic-assisted needle insertions: A robotic 7-degree-of-freedom arm (LBR iiwa, KUKA GmbH, Germany) performed planned stepwise needle insertions on seven tumors (Figure 2 Figure 3). Intraoperative CBCT imaging was used to track the displacement of the tumor- and the catheter markers. The targeting process for a single tumor began with the identification of the tumor's location on a CBCT image. Subsequently, the needle path was constructed based on specific criteria, including the shortest route, the avoidance of the tumor insertion path, and the extension of the path toward the catheter marker (the tumor is between the entry point and the catheter marker see Figure 4). Video-assisted guidance (ClarifEye, Philips Healthcare, Best, The Netherlands) was used to plan the needle path. ClarifEye is an augmented reality skin marker-based optical surgical navigation system that is connected to the Azurion system and supports needle path planning. During the procedure, the ClarifEye application provided a bullseye view to assist in positioning the robot arm (see Figure 3 and the Appendix VII. for a more detailed overview of the ClarifEye system).

A 13-gauge ablation needle (Emprint™ Percutaneous

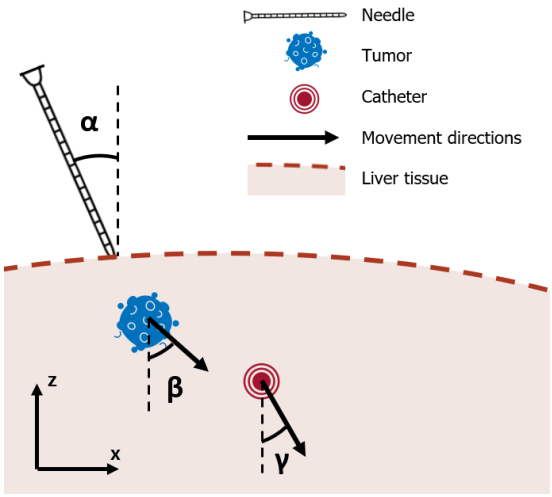

Figure 6: *Schematic overview of different angles during a needle insertion: the angle of the needle (α), the angle of the tumor (β), and the angle of the endovascular catheter marker (γ).*

Antennas - 25cm, Medtronic-Covidien, Minneapolis, United States) was positioned at the planned entry point, and the initial position of the markers was identified using a CBCT scan. The needle was then inserted into the tissue in small increments (5 mm) at a slow speed (0.01 m/s) using a programmed setting on the robot arm. After each insertion, a new CBCT scan was made to record the updated positions of the markers in space. This process of insertion and imaging was repeated five times until the needle tip reached the metal tumor marker. The targeting of a single tumor was repeated twice under the same conditions and along the same path.

2) Respiratory motion simulation: A medical infusion pump sachet (InfuseIT® Pressure Infusors, SunMed, Grand Rapids, United States) was used to simulate respiratory motion and initiate the soft tissue displacement. Based on the literature, a volume of 500 ml was chosen to mimic the lungs [36]. The sachet was positioned between the liver and the latex gloves (see Figure 5) and the displacement caused by respiratory motion was captured using CBCT scans at different stages of inflation (0%, 20%, 40%, 60%, 80%, and 100%). The experiment was performed once.

C. Data collection

The CBCT images (see Figure 4) were analyzed using an image viewer software application (dViewx64 version December 2022, Philips Healthcare, Best, The Netherlands) to determine the 3D coordinates of the tumor-, reference-, and catheter markers. The x- and y-directions correspond to the horizontal plane within the liver, and the z-direction corresponds to the vertical plane (see Figure 1). The coordinates of the markers were obtained by manually selecting them in the software and comparing them to the automatically generated coordinates, which were produced using a preprogrammed setting identifying high Hounsfield Unit values corresponding to the metal markers [37]. The coordinates were exported to Excel and calibrated using the reference marker and subtracting the coordinates. The figures were generated using MATLAB (version R2022a, The MathWorks, Inc., Natick, United States).

D. Data processing

The relationship between the tumor- and the catheter marker displacement during needle insertion is influenced by certain variables. In this explorative study, the influence of three independent variables was analyzed; the distance between the tumor- and the catheter marker, the insertion depth of the needle, and the insertion angle of the needle. The distance between the tumor- and the catheter marker was calculated using the Euclidean distance between the coordinates of the tumor center (the metal fiducial) and the coordinates of the radio-opaque marking on the endovascular catheter at the start of the experiment ($Euclidean\ distance = \sqrt{(x_1-x_2)^2+(y_1-y_2)^2+(z_1-z_2)^2}$. The needle insertion depth was the Euclidean distance traveled by the robot arm, according to the preprogrammed setting. The insertion angle of the needle was measured in the x-z plane using the image viewer software application (see Figure 6).

The independent variables in the respiratory motion simulation experiment were the distance between the tumor- and the catheter marker and the inflation volume of the medical sachet. The inflation volume of the medical sachet was controlled and measured with a manual pump connected to the sachet.

The dependent variables in both experiments were the displacement of the tumor- and catheter markers caused by the applied movement. In the needle insertion experiment, the angles of the tumor and catheter displacement were also dependent variables (see Figure 6). The displacement was used to calculate the following values: the overlap of the paths (%), the displacement range of the tumor markers (mm), and the offset (mm). The overlap of the paths was calculated as $overlap(\%) = (total path_{catheter}/total path_{tumor}) \cdot 100$, which indicates the similarity in the path between the tumor- and catheter marker. A value closer to 100 indicates a better overlap. The overlap was calculated for each individual tumor-catheter pair and also for the tumor-catheter groups based on distance. The average overlap of all tumor markers and catheter markers was calculated for each needle insertion and inflation step. The displacement range of the tumors was the average Euclidean path length of the tumors for each group of tumor-catheter pairs ($Avg.\ displacement = \Sigma^n path_{tumor}/n$). The offset, defined as the absolute value in millimeters of the discrepancy between the tumor- and catheter marker path, was calculated as $offset = path_{tumor} - path_{catheter}$. The offset between tumor- and catheter markers were either calculated per group based on the average total path, or calculated for all tumors and for all catheter markers for each needle insertion and inflation step.

In the needle insertion experiment, the following variables were controlled: the speed of insertion (0.01 m/s), the use of ClarifEye guidance, the type of ablation needle, the depth of the tumor in the tissue (which dictated the insertion depth of 25 mm), the types of markers used, the liver used, the number of repetitions of the targeting process. In the respiratory motion experiment, the following variables were controlled: the depth of the tumors in the tissue, the type of the inflatable sachet, the types of markers used, and the liver used (see Figure 7 for a schematic overview of both movements).

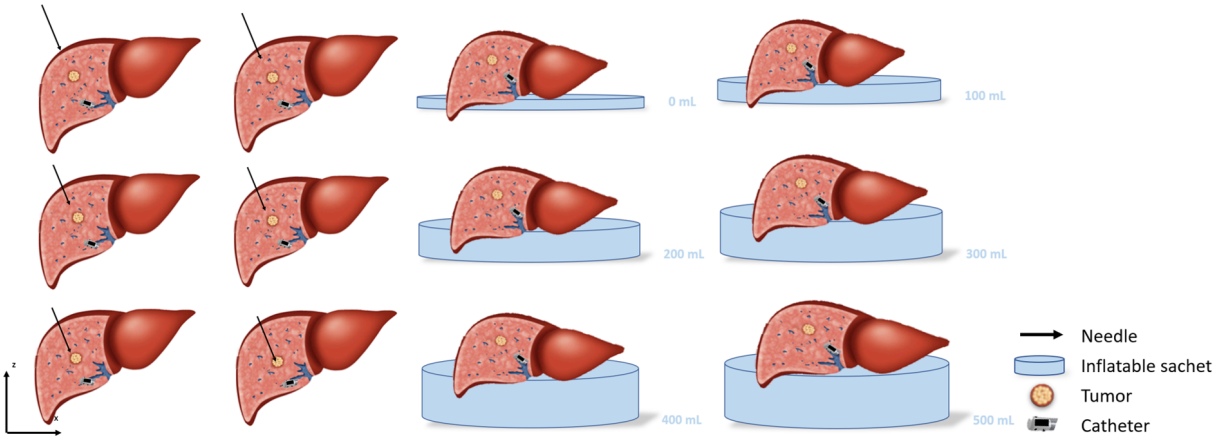

Figure 7: *The schematic displacement for the two experiments. F.l.t.r.: The schematic displacement of the needle, tumor-, and catheter marker during needle insertion. The needle was stepwise inserted 5mm into the liver until the needle arrived at the center point marked with the metal fiducial - The schematic displacement of the needle, tumor-, and catheter marker during respiratory motion. The inflatable sachet is stepwise inflated with +20 % (100 ml) of air.*

Table 1: *Characteristics of the tumor- and catheter marker relationship during needle insertion. The tumor-catheter marker pairs are sorted into 3 groups based on their Euclidean distance from each other at the beginning of the insertion. Per group, the overlap of the path* $(overlap(\%) = (path_{catheter}/path_{tumor}) \cdot 100)$*, the average displacement range of the tumors (average path lengths of the tumors), and the absolute value of the offset in mm are shown in the table* $(offset = path_{tumor} - path_{catheter})$*. The y-direction is excluded for needle insertion, as little to no displacement was recorded in this setup. The results show the lowest errors for catheters nearby the tumors (group 1) and the highest errors for catheters far away from the tumors (group 3), suggesting a relation between distance and overlap.*

Group	Tumor catheter pair	Distance to each other	X			Z			EUC		
			Overlap (%)	Avg. displacem. (mm)	Offset (mm)	Overlap (%)	Avg. displacem. (mm)	Offset (mm)	Overlap (%)	Avg. displacem. (mm)	Offset (mm)
Group 1	T6-C6	8.87	72.46	3.00	0.83	90.75	2.49	0.23	82.12	4.06	0.73
	T1-C1	9.46									
Group 2	T4-C4	12.66	49.92	1.98	0.99	52.50	5.89	2.80	49.65	6.79	3.42
	T7-C7	18.04									
	T5-C5	18.36									
Group 3	T2-C2	26.52	21.05	1.56	1.23	38.98	4.52	2.76	38.42	4.81	2.96
	T3-C3	27.67									

Table 2: *Characteristics of the tumor- and catheter marker relationship regarding the displacement during respiratory motion. Per group, the overlap of the path, the average displacement range of the tumors (average path lengths of the tumors), and the absolute value of the offset in mm are shown in the table. The values of T7-C7 are excluded (see Figure 14) and the y-values of T3-C3 are excluded (see Figure 15*

Group	Tumor catheter pair	Distance to each other	X			Y			Z			EUC		
			Overlap (%)	Avg. displacem. (mm)	Offset (mm)	Overlap (%)	Avg. displacem. (mm)	Offset (mm)	Overlap (%)	Avg. displacem. (mm)	Offset (mm)	Overlap (%)	Avg. displacem. (mm)	Offset (mm)
Group 1	T6-C6	7.96	188.90	1.97	0.66	59.23	5.56	2.29	98.26	24.77	0.24	95.69	25.70	0.73
	T1-C1	8.92												
Group 2	T5-C5	17.09	29.50	5.56	3.92	62.46	10.47	3.93	135.87	24.53	8.80	124.82	27.24	6.76
	T7-C7	18.63												
Group 3	T2-C2	27.18	183.60	3.68	3.62	23.59	5.31	4.00	88.27	28.84	4.28	86.42	29.58	4.48
	T4-C4	29.11												
	T3-C3	40.77												

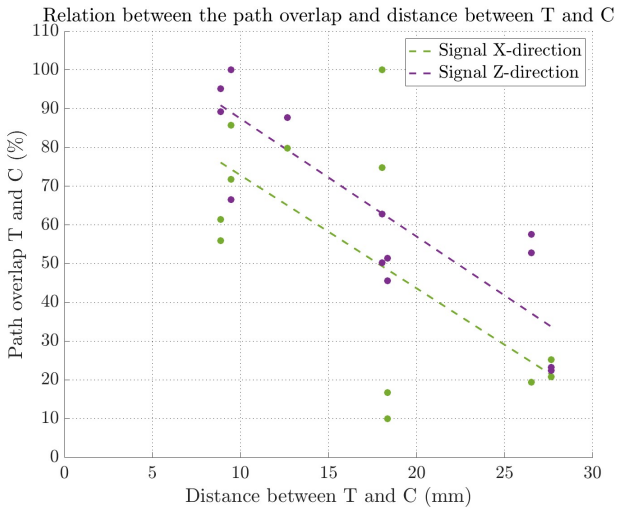

Figure 8: *The relation between the path overlap of the tumor and catheter ($overlap(\%) = (path_{catheter}/path_{tumor}) \cdot 100$) versus the distance between the tumor- and catheter marker during needle insertion. The data is split into the x-direction in green and the z-direction in purple (n=2 for each tumor). The higher trend line of the z-direction (purple) suggests a higher overlap on average compared to the x-direction (green).*

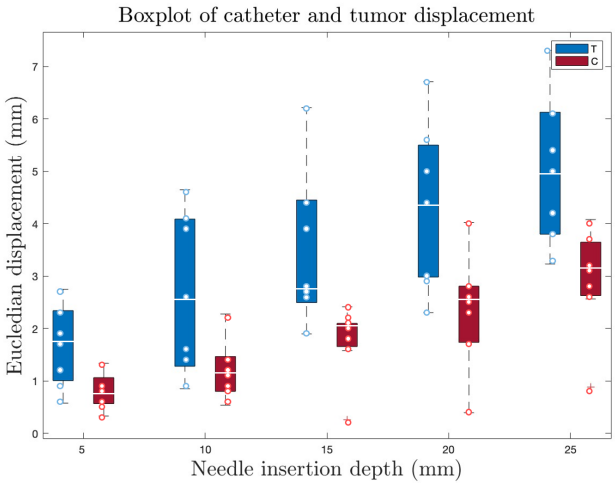

Figure 9: *Box plot on the Euclidean displacement of the tumors and catheters per each needle insertion step. The whiskers indicate the range of the data, the top of the box represents 75% of the data and the bottom 25% of the data, and the white line in the middle indicates the median. The individual data points are projected as an overlay on the box plot and represent the averaged value of two measurements (n=2).*

III. RESULTS

A. Robotic-assisted needle insertions

In the needle insertion experiment, we observed that all the tumor- and catheter markers underwent displacement (see Appendix VII.for all displacement plots). We will demonstrate the influence of the distance between the tumor and the catheter, the effect of the needle insertion depth, and the impact of the needle insertion angle.

1) The distance between the tumor and the catheter: The results showed the impact of increasing the distance between the tumor- and the catheter marker on the relationship between the tumor- and catheter marker displacement. This relationship, quantified as the percentage overlap, was calculated for three groups: group 1 (min-max 8-13 mm), group 2 (min-max 18-19 mm), and group 3 (min-max 26-28 mm) (see Table 1).

The results showed that as the distance between the tumor- and the catheter marker increased, the overlap of their paths in the x-, z-, and Euclidean directions decreased (see Table 1). The overlap in the z-direction was found to be the highest for all groups, compared to the x- and Euclidean directions (see Figure 8). The results suggested a bigger displacement in the z-direction (ranging from 2.49-5.89 mm) compared to the x-direction (ranging from 1.56-3.00 mm). The offset was also calculated for three groups in the x-, z-, and Euclidean directions. The maximum average offset in the x-direction was found to be 1.23 mm in group 3 (26-28 mm). In the z-direction, the maximum average offset of 2.80 mm was observed in group 2 (18-19 mm). In the Euclidean direction, the maximum average offset of 3.42 mm was observed in group 2 (18-19 mm). These results suggested that as the distance between the tumor and the catheter decreased, the overlap of the paths increased, with the z-direction displaying, on average, a higher overlap than the x-direction. However, the larger displacement in the z-direction also resulted in a higher offset. The results suggested that a catheter marker positioned in groups 1, 2, and 3 (8-28 mm) could be used to deduce the displacement of a tumor in the x-direction with a maximum average offset of 1.23 mm, while in the z- and Euclidean directions, a maximum average offset of 2.80 mm and 3.42 mm were already achieved in group 2 (18-19 mm).

Table 3: *The corresponding data to the box plot, calculating the mean for the tumors and catheters per needle insertion step, and the average offset per needle insertion step.*

Average Euclidean displacement (mm)				
Needle insertion depth	Tumor	Catheter	Average offset	Overlap (%)
5	1.60	0.71	0.89	44.60
10	2.68	1.13	1.55	42.15
15	3.47	1.48	1.99	42.56
20	4.29	1.98	2.31	46.21
25	5.03	2.51	2.52	49.94

2) The insertion depth of the needle: The results showed the effect of the needle insertion depth on the displacement of the tumor- and catheter markers: as the needle insertion depth increased, the displacement of the tumor- and catheter marker also increased (see Figure 9). The displacement of the tumors was greater and more variable than that of the catheter markers, as indicated by the larger boxes and longer whiskers in the data. The overlap showed a slight increase as the needle insertion depth increased, however, the average offset also increased from 0.89 mm for a 5 mm insertion to 2.52 mm for a 25 mm insertion (see Table 3).

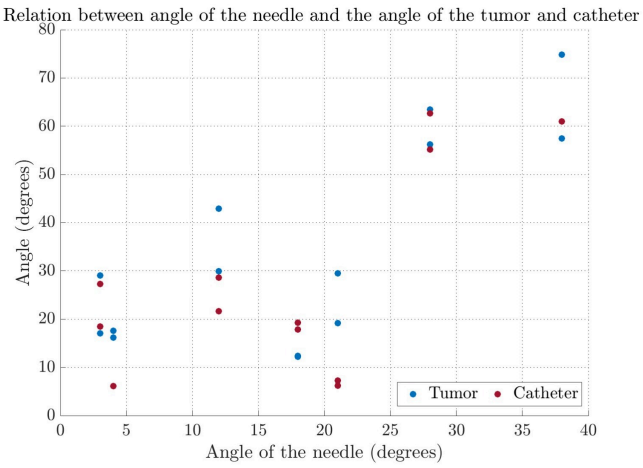

Figure 10: *The angle of the needle plotted against the angle of the tumor displacement and the catheter marker displacement. In red is the catheter marker angle and in blue is the tumor angle. The data points are for each target session separately (7 target sessions, with the same x-value), the data is not averaged (n=2). The variability between the 4 points with the same x-value indicates the difference between the displacement angle of the tumor- and catheter markers, the graph shows no clear increase or decrease in the variability.*

3) The insertion angle of the needle: In this study, the relationship between the angle of the needle and the angles of the tumor- and catheter marker displacement was shown (see Figure 6 for the angles). The data demonstrated no clear trend between the angle of the needle and the angles of the tumor- or catheter marker, nor a significant increase in variability between the tumor- and catheter marker as the angle of the needle increased (as shown in Figure 10). These findings suggest that the angles of the tumor- and catheter marker were not predictable based solely on the angle of the needle.

B. Respiratory motion simulation

During the respiratory motion simulation, we observed that all the tumor- and catheter markers underwent displacement (see Appendix VII. for all displacement plots). We will demonstrate the influence of the distance between the tumor and the catheter, and the effect of the inflation volume of the sachet.

1) The distance between tumor- and catheter marker: The results show for group 1 (7-9 mm) the lowest average offset for the x-, y-, z-, and Euclidean directions in comparison to group 2 (17-19 mm) and group 3 (27-41 mm) (see Table 2). However, the results suggest no clear pattern related to the percentage overlap and the distance between tumor- and catheter markers. This is substantiated by the scatter plot that showed no clear trend for x-, y-, or z-direction (see Figure 11). The widespread scatter plot indicates that the distance between the tumor and the catheter marker has no direct influence on the path overlap.

2) The inflation volume of the sachet: The impact of inflating the sachet on the relationship between the tumor- and the catheter marker was demonstrated. The results showed an increase in the average Euclidean displacement of the tumor-

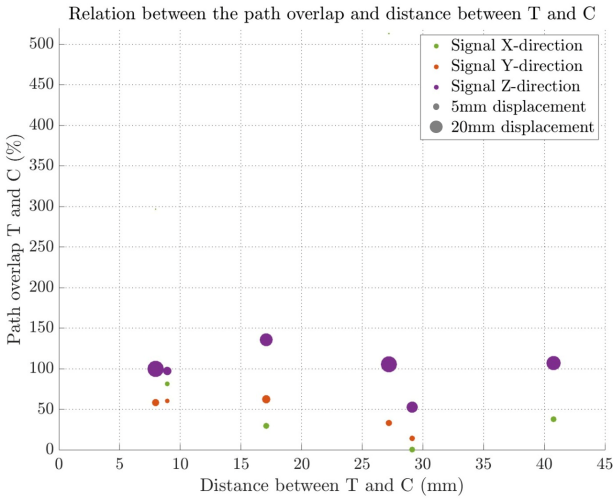

Figure 11: *The distance between tumor- and catheter marker plotted against x-, y-, and z-direction overlap of the catheter and tumor (n=1). The size of the data points represented the size of the displacement of the tumor. The z-direction movements were on average bigger (min-max 10.46-39.08 mm) than the x-direction (min-max 0.33-5.56) or the y-direction (min-max 3.27-10.47 mm). The z-direction showed overlap values closest to 100% (min-max 52.73-135.87%), and the x-direction (min-max 0.05-513.07%) and y-direction (min-max 13.89-62.46%) mainly the outliers. An extreme value; (27, 513) is a very small movement, and therefore less relevant. The data point of T7 is excluded as it was not exposed to a respiratory motion properly (Figure 14).*

and the catheter marker as the inflation volume increased (see Figure 12). It can be seen that the catheter has higher median values (for all inflation steps) and higher average displacements (after 40% inflation) compared to the tumors. When $path_{catheter} > path_{tumor}$, this resulted in an overlap percentage above 100% (see Table 4). The average offset increased from 0.05 mm for 20% inflation to a maximum of 0.84 mm at 80% inflation. These results suggested a positive correlation between inflation volume, displacement, and offset, with the catheter on average having a slightly larger displacement than the tumors.

IV. DISCUSSION

A. Observations from results

This work aims to improve the intraoperative guidance during a PNP in the liver, by making the first attempt at the usage of endovascular catheter markers to track the tumor displacement while the liver is being displaced by needle insertion or respiratory motion. An ex-vivo porcine liver with seven created tumor markers and four endovascular catheters with radio-opaque markings were used to track the displacement and observe the relationship between the tumor- and endovascular catheter markers. First, the results will be discussed and interpreted. Second, the limitations of this study will be addressed. Finally, future research areas will be discussed that can further increase the insights into soft tissue deformations in the liver during a PNP.

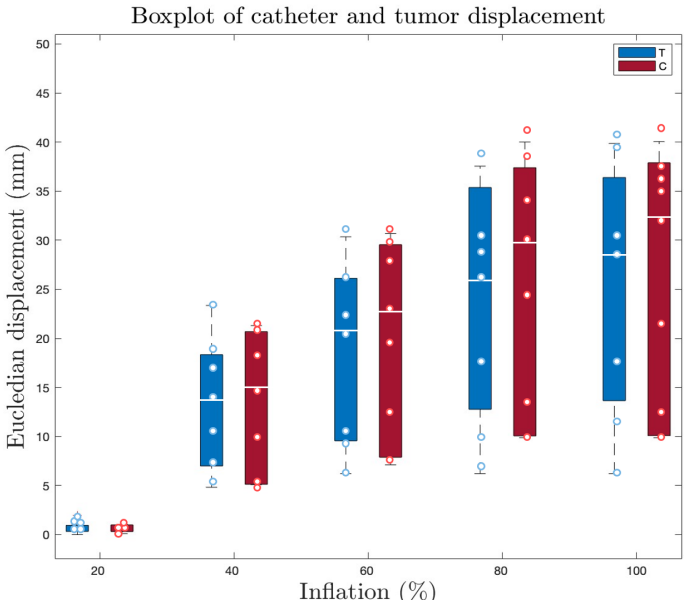

Figure 12: *Box plot on the Euclidean displacement of the tumors and catheter markers per each inflation step. The individual data points are overlayed (n=1).*

Table 4: *The corresponding to the box plot, calculating the mean for the tumors and catheter markers per inflation step, and the average offset (absolute value) per inflation step.*

Average Euclidean displacement (mm)				
Inflation (%)	Tumor	Catheter	Average offset	Overlap (%)
20	0.72	0.67	0.05	92.74
40	13.62	13.45	0.17	98.74
60	18.78	19.19	0.40	102.15
80	23.97	24.82	0.84	103.51
100	24.80	25.11	0.31	101.26

1) Robotic-assisted needle insertions insertion: The relationship was analyzed based on the distance between the tumor and the catheter marker, the insertion depth of the needle, and the insertion angle of the needle.

All seven tumor- and catheter markers showed displacement during the needle insertion. The relationship between the tumor- and catheter marker is expressed in the overlap, the closer to 100%, the better. The results showed a higher overlap for catheter markers that are nearby the tumor in the x-, z-, and Euclidean directions (see Figure 8 and Table 1). It can be concluded that a small distance between the tumor and catheter has a positive impact on the relation, as the force of the needle would have a more similar impact on the two markers when they are close to each other. This is also in line with previous research indicating that the accuracy of capturing tumor displacement decreases with increasing distance between implanted markers and the tumor [38]. Additionally, the average overlap (trend line) for the z-direction was higher (as shown in Figure 8). This can be explained by the fact that the catheter is aligned with the applied deformations in the z-direction, suggesting that a catheter is needed in every plane to achieve more accurate

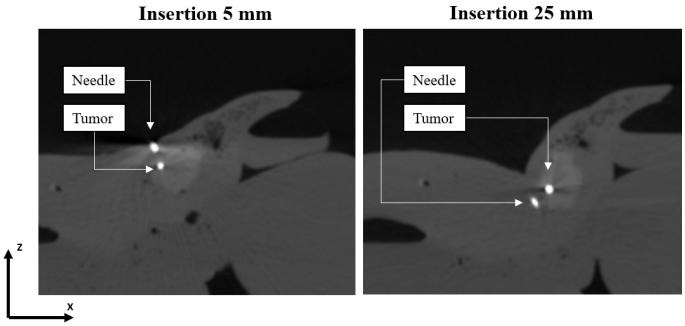

Figure 13: *The push away effect shown in the trial experiment. The left picture is at a needle insertion of 5 mm; the needle seems to target the tumor. The right picture is at a needle insertion of 25 mm; the needle misses the tumor. The planned path differs from the actual path.*

coverage for x-, y-, and z-displacement. This idea of using markers in multiple planes is also supported by the study of Beddar et al. [11]. In this research, the overlap percentages for the z-direction were higher than those for other directions. The average displacement ranges for the z-direction were also larger, leading to a greater offset and less accurate results in terms of millimeters. According to a previous study [23] and physicians, an accuracy margin of 2.00 mm is necessary for using a marker to accurately deduce the tumor displacement. Based on this criterion, the catheter marker can accurately determine tumor displacement in the x-direction for groups 1 (8-13 mm), group 2 (18-19 mm), and group 3 (26-28 mm), and in the z- and Euclidean directions only for group 1 (8-13 mm). The data demonstrated a positive correlation between the depth of needle insertion and the Euclidean displacement for all tumors and catheters (Figure 9). As the depth of insertion increased, the displacement also increased, resulting in an offset that exceeded the 2.00 mm accuracy threshold for depths greater than 15 mm. Even though, the overlap percentage showed a slight increase after 15 mm insertion depth (Table 1). Thus, in this experimental setup, the relationship between the tumor- and catheter markers was relatively consistent in terms of overlap, but the magnitude of the offset increased with the depth of insertion due to the increase in displacement for both the tumor- and catheter markers. It is expected that the increase in displacement may be attributed to the slow insertion technique and can be decreased by adjusting the insertion technique. Previous research, by Sugiyama et al. [32], has demonstrated that an accelerated needle insertion leads to less organ displacement. This concept is also supported by the study by Gao et al. [12], which found that displacement decreases with an increase in insertion velocity due to the increased kinetic and dissipated energies generated at higher velocities. Therefore, in this experimental setup, the catheter marker can accurately deduce the displacement of the tumor for a maximum needle insertion depth of 15 mm with the current slow insertion technique.

The results of this study indicated that the angle of the needle had no clear relatable effect on the resulting angles of the tumor- and catheter displacement (Figure 10). A potential explanation for the unpredictable tumor angle could be the position of the FM within the agar sphere. It was not confirmed during the experiment whether the FM was located

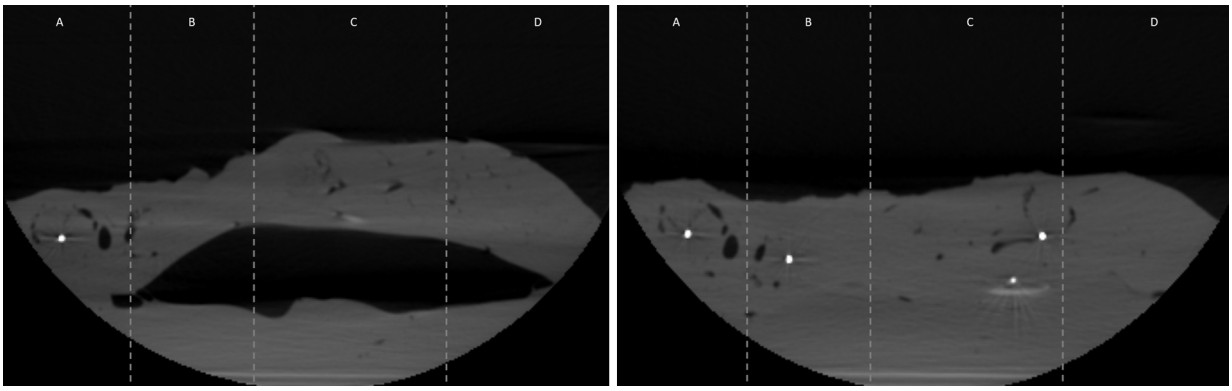

Figure 14: *Inflation of the sachet. F.l.t.r: Inflation of 60% with in black the inflatable, and the white dot is T7. The figure shows four zones (A, B, C, and D) that each experience a different inflation magnitude. A is outside the blow zone, B is subjected to the incline of the sachet with a big variability, C is rather constant, and D is the decline of the sachet. T7 is located in zone A, while the catheter is located in a different blow zone (B) of the inflatable sachet, and therefore not taken into account in the results. - Right picture shows inflation of 0%, this clearly shows that T7 is not influenced properly by the inflation sachet, the catheter marker is not shown since it is on a different CBCT slice.*

exactly in the center of the agar sphere. As a result, it is possible that the needle targeted the FM on the outer side of the sphere, causing the sphere to be pushed sideways rather than directly puncturing it Figure 13. While this scenario may not be relevant in a clinical setting, as there will be no marker present, it is important to aim for the center of the tumor in order to minimize displacement. Furthermore, in the scenario where the sphere is pushed sideways, the actual needle path deviated from the planned needle path. This deviation was not analyzed in this study, as the focus was on the deformation of soft tissue. However, in a clinical setting, quantifying this deviation may be important as it may affect the accuracy of needle insertion.

A potential explanation for the unpredictable angle of endovascular catheter markers could be the orientation of the entire catheter relative to the applied needle force (e.g. perpendicular or parallel orientation). This orientation could affect the reaction force and, therefore, the angle of the displacement of the catheter markers. Another potential explanation for the unpredictability of both the tumor- and the catheter markers is the in-homogeneity of the liver structure. Local structures like bile ducts and small blood vessels can obstruct paths and therefore influence the eventual direction of the displacement [35]. In conclusion, the angle of the tumor- and catheter marker displacement cannot be predicted based solely on the angle of the needle insertion. It depends on more factors like the specific orientation of the FM in the agar sphere, the catheter orientation, and the local structures in the liver.

2) Respiratory motion simulation: During the respiratory motion experiment, the relationship was analyzed based on the following variables; the distance between the tumor and the catheter, and the inflation of the sachet.

The results of the study indicated no clear correlation between the distance between the tumor and the catheter and the overlap of their paths (Figure 11). The results showed that the displacement range of the tumor in the z-direction (min-max 10.46-39.08 mm) was greater than in the x- (min-max 0.33-5.56) or y-direction (min-max 3.27-10.47 mm), and that the overlap values were also closer to 100% in the z-direction. This suggests that the z-direction movements were most influential and had the greatest influence on the overlap of the catheter and tumor path. This was expected since the inflatable sachet moves mainly in the z-direction. Furthermore, when looking at the z-direction data alone (Figure 11), it becomes even more evident that there was no trend between the path overlap and the distance between the tumor- and catheter marker during respiratory activity. This lack of correlation can be attributed to the uniform force applied by the inflation sachet, which resulted in similar displacements for points, independent of the distance between the points. The variations observed in the data for different tumors may be explained by differences in the "blow zone," which is defined as the area affected by the inflated sachet (Figure 14). When a tumor was located in a different zone than the catheter it was matched to, this led to unreliable results. In a human body, the "blow zone" would emphasize the importance of being on the same sagittal slice (a longitudinal plane that divides the body into right and left sections) and coronal slice (a frontal plane that divides the body into front and back sections), rather than the axial slice (a horizontal plane that divides the body into superior and inferior sections). To conclude, the overlap of the tumor and catheter paths were not primarily influenced by the distance between the two points, but rather by the blow zone in which they were located. In a human body, this would suggest positioning the catheter marker on the same sagittal and coronal slice.

The results of this study indicated that an increase in the volume of inflation of a sachet led to an increase in the displacement of both tumor- and catheter markers (Figure 12). This was a predictable outcome given that the sachet applied a uniform force. On average, the Euclidean offset per inflation step for all tumors and catheters was relatively small, ranging from 0.05 to 0.84 mm (Table 4). This suggests that the seven tumors and catheters generally exhibit similar behavior in this experimental setup. However, when analyzing the average Euclidean offset per tumor-catheter pair group, the offset varies from 0.73 to 6.76 mm (Table 2). This indicates that there is a discrepancy between the pairs, which may be due to

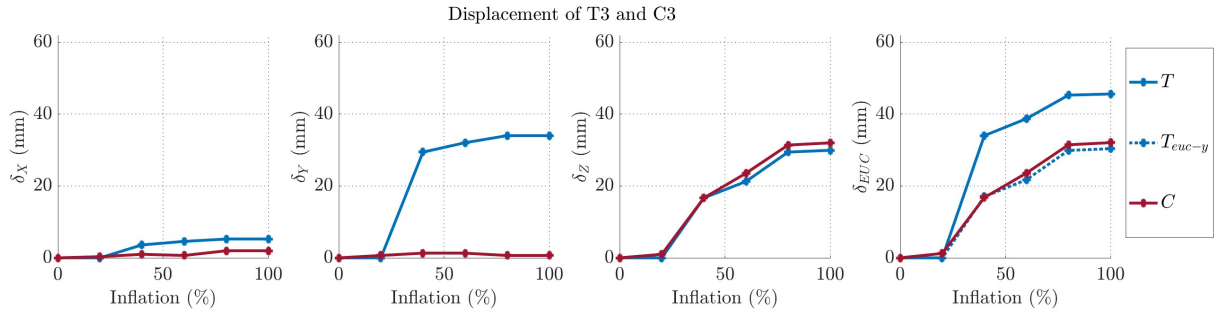

Figure 15: *The displacement of T3. Showing the inflation % on the x-axis and the displacement in mm for the x-, y-, z-, and Euclidean direction of the y-axis (n=1).*

the fact that the pairs are now matched based on the distance between the markers rather than the blow zone. Overall, these results suggest that in this experimental setup, a catheter can provide an average displacement accuracy of the tumor within 2.00 mm until an inflation volume of 500 ml.

B. Limitations of the study

The ex-vivo liver tissue used in the study simulated a realistic setting, but certain limitations should be taken into consideration when interpreting the results. First, the ex-vivo liver used in this study was from a pig. The lobes of a pig liver are individual segments connected by small ligaments at the proximal side, while a human liver is considered to be a single piece. The lobes of the liver have the ability to exhibit a gliding effect due to their incomplete connection and can move horizontally over the sachet. This led to a significant displacement of 29.42 mm for T3 when inflating from 20 to 40% (as shown in Figure 15). The individual segments also created a thin and flat tissue compared to the thicker piece of a human liver. The anatomical differences might have resulted in a deformation that is clinically unrealistic, so it is essential to compare the results with those obtained from an (ex-vivo) human liver.

Second, the tissue characteristics of the liver can vary depending on the patient's lifestyle, with cirrhotic livers being harder than healthy livers. This experiment was performed on a healthy pig liver (relatively soft). However, according to the American Cancer Society, "most (but not all) people who develop liver cancer already have some evidence of cirrhosis" [39]. This suggests that the results obtained from a healthy pig liver may not be representative of the average patient undergoing percutaneous needle procedures for hepatic cancer treatment.

Third, the agar used in this study to mimic the tumor has several limitations when compared to a real tumor. For instance, the agar cannot replicate the hard shell that encapsulates a tumor. A softer outer shell might decrease the influence of the push-away effect compared to the current model. Furthermore, the shape of the agar sphere is difficult to control; depending on the local liver structure, the agar might also dissipate into a bile duct instead. Additionally, the placement ad the movement of the FM marker within the agar is hard to control and impacts the results of the push-away effect. In this setup, it is unclear whether the FM moved in the agar sphere or whether the FM moved together with the agar sphere.

Fourth, there are a few limitations regarding the radio-opaque markings on the catheter that were used as endovascular markers. The fixation of the catheter was assessed at the start of the experiment by applying deformations and confirmed to be stable. However, it can be seen in Table 1 and Table 2 that there has been a displacement of catheter 2 (with markings C3 and C4): the distance between T3-C3 was 27.67 mm and increased with 13.10 mm to 40.77 mm, the distance between T4-C4 was 12.66 mm and increased with 16.45 mm to 29.11 mm. This implies that the catheter moved in between the two experiments. It is uncertain how this may have changed during the experiment. Although, it is hypothesized that it did not influence the results due to the similarity in displacement values observed for each experiment. However, it should be noted that this study has the limitation of not using endovascular markers that are directly fixed into the veins without being attached to a catheter.

Fifth, the applied deformations (both needle insertion and the respiratory motion) were static, as live imaging and tracking were not possible. However, it is known that organ surface deformation is a dynamic process that includes multiple phases, such as deformation, steady penetration, and relaxation [12]. It is a limitation of the study that these multiple phases were not taken into account.

Sixth, the respiratory motion was simulated with an inflatable sachet whose volume was regulated and measured using a manual pump. However, the accuracy of this measurement could be improved by implementing an automatically controlled barometer.

Seventh, the same ablation needle was used throughout the entire experiment, which may have resulted in a decrease in sharpness over time. This could impact the puncture or pushing away effect of the tumor, as a sharp needle is more likely to puncture the tissue while a blunt needle is more likely to push it away [40]. This should be considered in future studies.

Eight, the needle insertion experiment did not consider displacement in the y-direction due to the minimal displacement in this direction. This resulted in the angle measurement of the needle being recorded in two dimensions (x- and z-directions) rather than three, which may potentially impact the accuracy and comprehensiveness of the analysis and conclusions drawn from the experiment.

Ninth, for the needle insertion experiment, the measurements

were repeated twice under the same conditions with the same planned trajectory. The needle's prior passage through the tissue might influence the deformation. Using a phantom, in which the tissue is reversible, could potentially eliminate this source of variability in the deformation measurements. Overall, the limitations of this study suggest that caution should be exercised in generalizing the findings to other contexts, and further research is needed to address these limitations and expand upon the current knowledge of soft tissue deformation during a PNP in the liver.

C. Future work

The current study can be improved by considering several factors in future research. First, regarding the ex-vivo porcine liver model; the number of endovascular markers per tumor needed should be determined by examining the results when using a marker in the x-, y-, and z-plane. The results of Section 1) and Beddar et al. [11] suggest this will improve the accuracy margins. Furthermore, the exact location of the markers should be determined, such as in the hepatic arteries or veins. Also, the variable of tumor depth in tissue should be varied in order to better understand the factors influencing the relationship between tumor-catheter displacement. Moreover, it would be of added value to assess more tumors and to have an endovascular marker every millimeter around a tumor. This will strengthen the range definition for an accurate endovascular marker. Next, the predictability of the angle of the tumor- and catheter displacement should be looked into; by further examining the positioning of the FM in the agar sphere, looking into the orientation of the catheter, and investigating the influence of local structures in the liver.

Second, regarding the applied deformations of needle insertion and respiratory activity; the needle insertion techniques should be varied by adjusting the speed and step size. Moreover, the inflation sachet used in the respiratory experiment should be at least the same size as the liver to prevent tumors or catheters from being outside the "blow zone" and not provide representative inflation data. To further expand the research, it would be of added value if the needle insertion and respiratory motion would be combined, and the deformation caused by patient repositioning would be added. In conclusion, these suggestions could contribute to a more realistic scenario, bringing the usage of endovascular markers closer to clinical implementation.

V. CONCLUSION

The aim of this explorative study was to gain insights into the soft tissue deformation in the liver during a percutaneous needle procedure (PNP) and evaluate the potential for using an endovascular catheter marker to capture tumor displacement. The primary causes of soft tissue deformation that arise during a PNP are needle insertion and respiratory motion. An ex-vivo porcine liver was used to study the soft tissue deformation. The factors that influence the relationship between the tumor- and catheter marker displacements during needle insertion are the distance between the tumor- and the catheter marker and the needle insertion depth. The results demonstrated the ability of a catheter marker to accurately deduce tumor displacement in the x-direction within a range of 0-28 mm around the tumor and in the z- and Euclidean directions within a range of at least 0-13 mm around the tumor. The catheter marker could also be used to deduce tumor displacement during needle insertion up to a maximum insertion depth of 15 mm with the current slow (0.01 m/s) insertion technique. The impact of the angle of needle insertion on tumor and catheter displacement was also examined, but the results showed that it was not possible to solely use the angle of needle insertion to predict the angle of displacement. It is likely that the angle of tumor and catheter displacement is influenced by a combination of other factors such as the specific orientation of the marker in the agar sphere, the orientation of the catheter, and local structures in the liver. The factors that influence the relationship between the tumor- and catheter marker displacements during respiratory motion are the location of the tumor- and the catheter marker in the same sagittal and coronal plane in the liver and the inflation volume of the sachet. This study found that the overlap of the tumor- and catheter paths were not primarily influenced by the distance between the two markers, but rather by the blow zone in which they were located. On average, the catheters were able to provide tumor displacement information in this setup for an inflation volume of 0-500 ml (100%). The results suggest the importance of positioning the endovascular marker in the same blow zone as the tumor, in the human body, this would imply having the marker in the same sagittal and coronal plane as the tumor. Further research is needed to confirm these findings and determine their clinical applicability. This should include tracking the displacement of a greater quantity of tumors and catheter markers, examining a variety of tumor depths in the tissue, and evaluating a broader range of distances between the tumor and catheter. This study contributed to a better understanding of the soft tissue deformations in a liver during a percutaneous needle procedure by studying the impact of the needle insertion and respiratory motion.

VI. ACKNOWLEDGEMENT

The present article is a partial fulfillment of the requirements for the Master of Science in Biomedical Engineering at the Delft University of Technology. The corresponding author expresses her gratitude to the supervisors, Dr. Dodou, P. Goossen-Nachtigall, and Dr. A.H. Muris, for their valuable guidance and support throughout the course of this work. Their contributions are greatly appreciated.

References

[1] Ricardo Robles-Campos et al. “Open versus minimally invasive liver surgery for colorectal liver metastases (LapOpHuva): a prospective randomized controlled trial”. In: *Surgical endoscopy* 33.12 (2019), pp. 3926–3936.

[2] John R Leyendecker and Gerald D Dodd III. “Minimally invasive techniques for the treatment of liver tumors”. In: *Seminars in liver disease*. Vol. 21. 02. Copyright© 2001 by Thieme Medical Publishers, Inc., 333 Seventh Avenue, New ... 2001, pp. 283–292.

[3] Danny de Lange. “Technology assessment and usability study of a steerable needle prototype as a tool in assisting percutaneous liver interventions”. In: (2019).

[4] J.C. Hogervorst. *Percutaneous measurement of tissue compliance*. Jan. 1970. URL: http://resolver.tudelft.nl/uuid:2f21f9e7-5f92-4da1-9624-a68e15bec0fb.

[5] T.P. Pusch. *From the wasp ovipositor to a 3D steerable needle for solid-tissue interventions: A design and experimental approach*. Jan. 1970. URL: http://resolver.tudelft.nl/uuid:086fc121-5e50-48cd-9dd0-af4da7fa96c2.

[6] Marta Scali. “Self-propelling needles: From biological inspiration to percutaneous interventions”. In: (2020).

[7] Lee W Goldman. “Principles of CT: radiation dose and image quality”. In: *Journal of nuclear medicine technology* 35.4 (2007), pp. 213–225.

[8] S Vijayalakshmi et al. “Image-Guided Surgery Through Internet of Things”. In: *Internet of Things in Biomedical Engineering*. Elsevier, 2019, pp. 75–116.

[9] Chiara Floridi et al. “Precision Imaging Guidance in the Era of Precision Oncology: An Update of Imaging Tools for Interventional Procedures”. In: *Journal of Clinical Medicine* 11.14 (2022), p. 4028.

[10] Junichi Tokuda et al. “Motion compensation for MRI-compatible patient-mounted needle guide device: estimation of targeting accuracy in MRI-guided kidney cryoablations”. In: *Physics in Medicine & Biology* 63.8 (2018), p. 085010.

[11] A Sam Beddar et al. “Correlation between internal fiducial tumor motion and external marker motion for liver tumors imaged with 4D-CT”. In: *International Journal of Radiation Oncology* Biology* Physics* 67.2 (2007), pp. 630–638.

[12] Dedong Gao, Yong Lei, and Bin Yao. “Dynamic soft tissue deformation estimation based on energy analysi”. In: *Chinese Journal of Mechanical Engineering* 29.6 (2016), pp. 1167–1175.

[13] Shamel Fahmi, Frank FJ Simonis, and Momen Abayazid. “Respiratory motion estimation of the liver with abdominal motion as a surrogate”. In: *The International Journal of Medical Robotics and Computer Assisted Surgery* 14.6 (2018), e1940.

[14] Tonke L de Jong. “Needles and liver phantoms in interventional radiology: Design considerations”. In: (2019).

[15] Marieke van Dommele. *NARRATIVE REVIEW ON IMAGE-GUIDED THERAPY AND SOFT-TISSUE TRACKING DURING PERCUTANEOUS NEEDLE PROCEDURES IN THE ABDOMEN*. 2022.

[16] Cheng Li et al. “Subject-specific and respiration-corrected 4D liver model from real-time ultrasound image sequences”. In: *Computer Methods in Biomechanics and Biomedical Engineering: Imaging & Visualization* 6.1 (2018), pp. 7–16.

[17] Minglei Yang et al. “Ultrasound fusion image error correction using subject-specific liver motion model and automatic image registration”. In: *Computers in biology and medicine* 79 (2016), pp. 99–109.

[18] G Vashistha. “Robot assisted needle positioning system for liver biopsy”. MA thesis. University of Twente, 2021.

[19] Aurora Fassi et al. “Tumor tracking method based on a deformable 4D CT breathing motion model driven by an external surface surrogate”. In: *International Journal of Radiation Oncology* Biology* Physics* 88.1 (2014), pp. 182–188.

[20] Lai-Lei Ting et al. “Tumor motion tracking based on a four-dimensional computed tomography respiratory motion model driven by an ultrasound tracking technique”. In: *Quantitative Imaging in Medicine and Surgery* 10.1 (2020), p. 26.

[21] Tengfei Wang et al. “Patient specific respiratory motion model using two static CT images”. In: *Proceedings of the 2nd International Symposium on Artificial Intelligence for Medicine Sciences*. 2021, pp. 488–492.

[22] Yusuf Özbek, Zoltán Bárdosi, and Wolfgang Freysinger. “respiTrack: Patient-specific real-time respiratory tumor motion prediction using magnetic tracking”. In: *International Journal of Computer Assisted Radiology and Surgery* 15.6 (2020), pp. 953–962.

[23] Boris Guiu et al. “Feasibility, safety and accuracy of a CT-guided robotic assistance for percutaneous needle placement in a swine liver model”. In: *Scientific reports* 11.1 (2021), pp. 1–11.

[24] Esther ND Kok et al. “Accurate surgical navigation with real-time tumor tracking in cancer surgery”. In: *NPJ precision oncology* 4.1 (2020), pp. 1–7.

[25] Melina Kord et al. “Risks and Benefits of Fiducial Marker Placement in Tumor Lesions for Robotic Radiosurgery: Technical Outcomes of 357 Implantations”. In: *Cancers* 13.19 (2021), p. 4838.

[26] Egidijus Pelanis et al. “Evaluation of a novel navigation platform for laparoscopic liver surgery with organ deformation compensation using injected fiducials”. In: *Medical image analysis* 69 (2021), p. 101946.

[27] Lena Maier-Hein et al. “On combining internal and external fiducials for liver motion compensation”. In: *Computer Aided Surgery* 13.6 (2008), pp. 369–376.

[28] Willem Hoitzing. *Respiratory Motion Modelling in the Liver: Tumour Motion Prediction for Robot-Assisted Needle Guidance*. Apr. 2019.

[29] Marco Solbiati et al. “Thermal Ablation of Liver Tumors Guided by Augmented Reality: An Initial Clinical Experience”. In: *Cancers* 14.5 (2022), p. 1312.

[30] Deqiang Xiao et al. “In vivo comparison of two navigation systems for abdominal percutaneous needle intervention”. In: *Abdominal Radiology* 42.7 (2017), pp. 1993–2000.

[31] Cornel Zachiu et al. “Real-time non-rigid target tracking for ultrasound-guided clinical interventions”. In: *Physics in Medicine & Biology* 62.20 (2017), p. 8154.

[32] Kojiro Sugiyama. *Accelerated puncture into kidney phantom*. confidential document.

[33] Andriy Nykonenko. *Anatomic Peculiarities of Pig and Human Liver*. URL: http://www.ectrx.org/detail/archive/2017/15/1/0/21/0.

[34] Lei Zhang et al. “A tactile sensor for measuring hardness of soft tissue with applications to minimally invasive surgery”. In: *Sensors and Actuators A: Physical* 266 (2017), pp. 197–204.

[35] Katrien Vekemans and Filip Braet. “Structural and functional aspects of the liver and liver sinusoidal cells in relation to colon carcinoma metastasis”. In: *World Journal of Gastroenterology: WJG* 11.33 (2005), p. 5095.

[36] Adem Gölcük and İnan Güler. “The use of stepper motor-controlled proportional valve for fio2 calculation in the ventilator and its control with fuzzy logic”. In: *Journal of medical systems* 41.1 (2017), pp. 1–10.

[37] Tami D DenOtter and Johanna Schubert. “Hounsfield Unit”. In: (2019).

[38] Yvette Seppenwoolde et al. “Treatment precision of image-guided liver SBRT using implanted fiducial markers depends on marker–tumour distance”. In: *Physics in Medicine & Biology* 56.17 (2011), p. 5445.

[39] *Liver cancer causes risk factors and prevention*. URL: www.cancer.org/content/dam/CRC/PDF/Public/8699.00.pdf.

[40] *Microcannula vs. Sharp Tip Needles Advantages and disadvantages - face medical supply*. Dec. 2022. URL: https://facemedstore.com/blogs/blog/microcannula-vs-sharp-tip-needles-advantages-and-disadvantages.

A

Displacement plots of tumor and catheter

A.1. Needle insertion

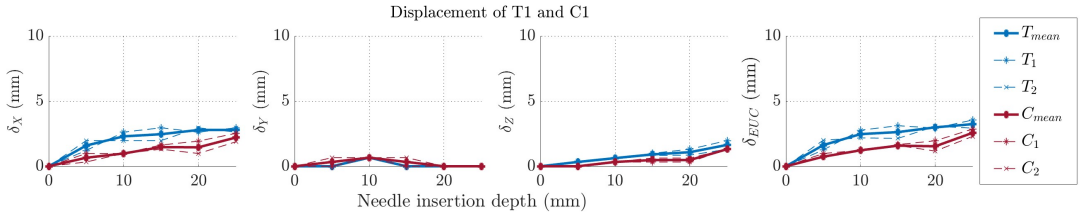

Figure A.1: *The displacement of T1 and its catheter. Based on 2 measurements*

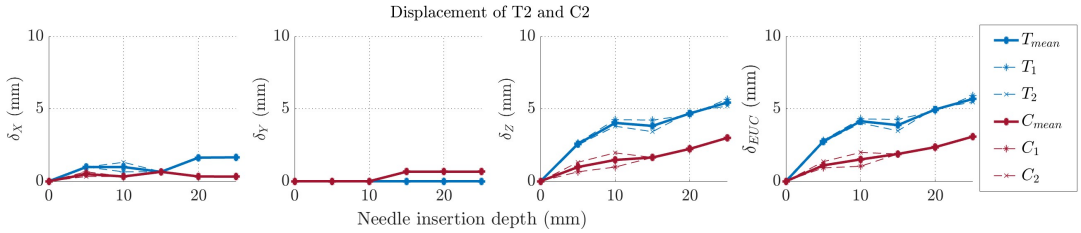

Figure A.2: *The displacement of T2 and its catheter. Based on 2 measurements*

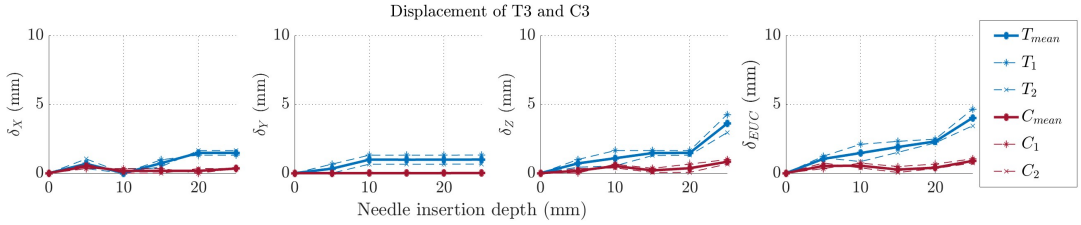

Figure A.3: *The displacement of T3 and its catheter. Based on 2 measurements*

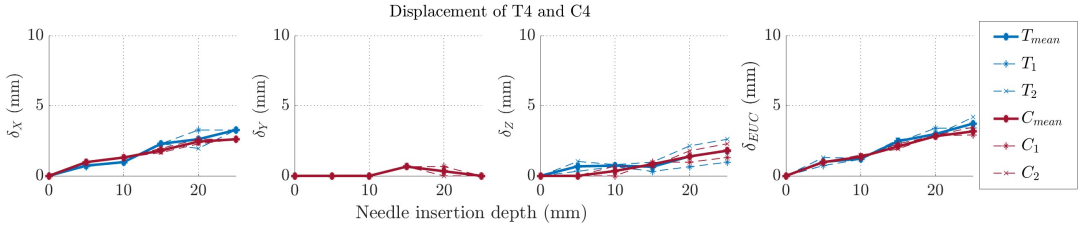

Figure A.4: *The displacement of T4 and its catheter. Based on 2 measurements*

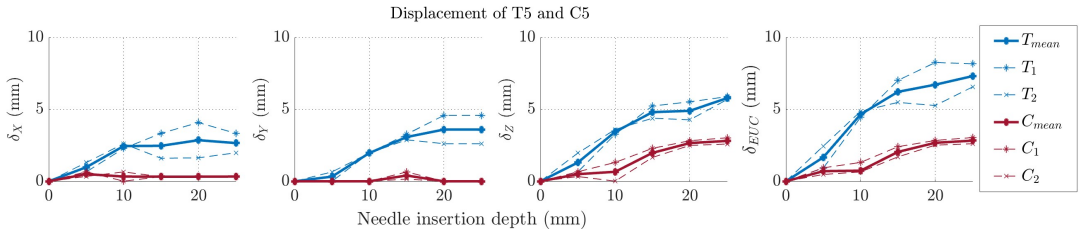

Figure A.5: *The displacement of T5 and its catheter. Based on 2 measurements*

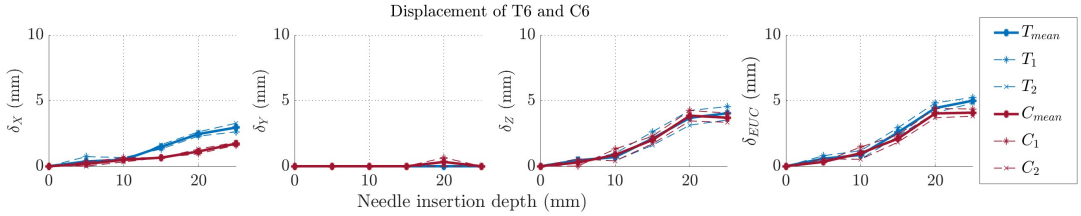

Figure A.6: *The displacement of T6 and its catheter. Based on 2 measurements*

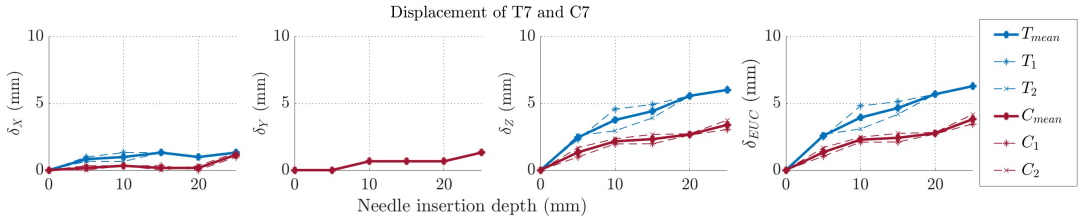

Figure A.7: *The displacement of T7 and its catheter. Based on 2 measurements*

A.2. Respiratory activity

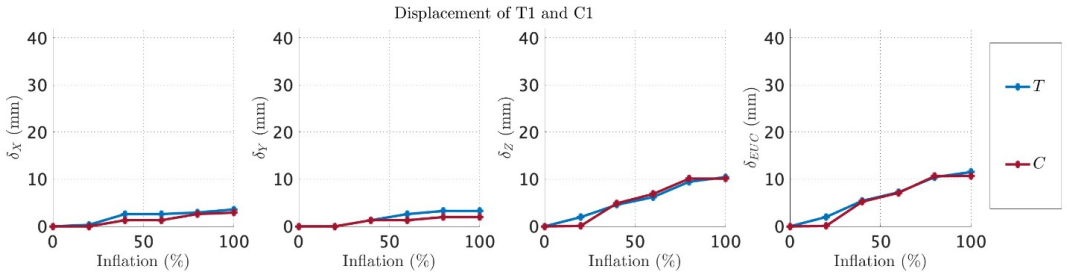

Figure A.8: *The displacement of T1 and its catheter. Based on 1 measurement*

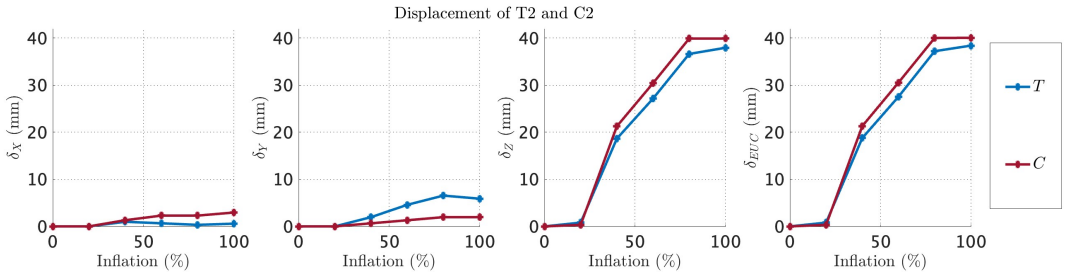

Figure A.9: *The displacement of T2 and its catheter. Based on 1 measurement*

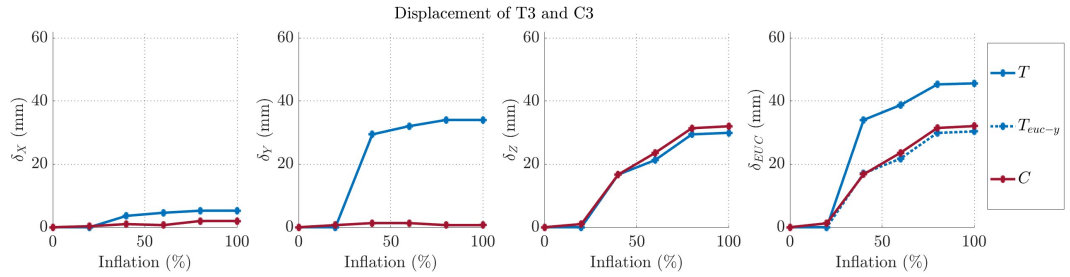

Figure A.10: *The displacement of T3 and its catheter. Based on 1 measurement*

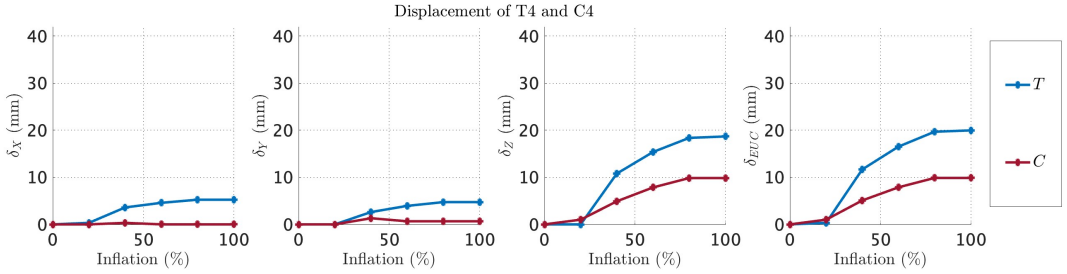

Figure A.11: *The displacement of T4 and its catheter. Based on 1 measurement*

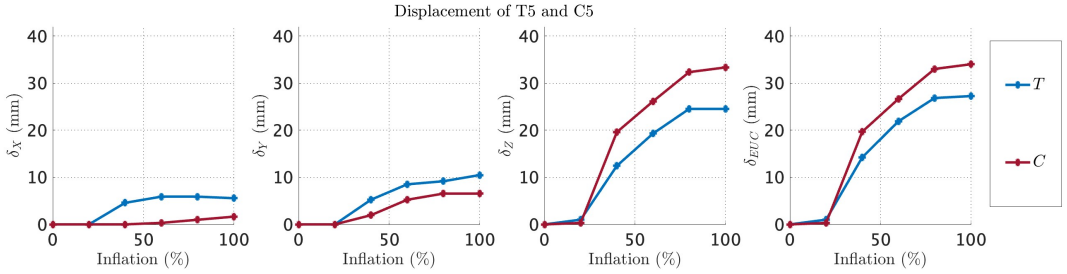

Figure A.12: *The displacement of T5 and its catheter. Based on 1 measurement*

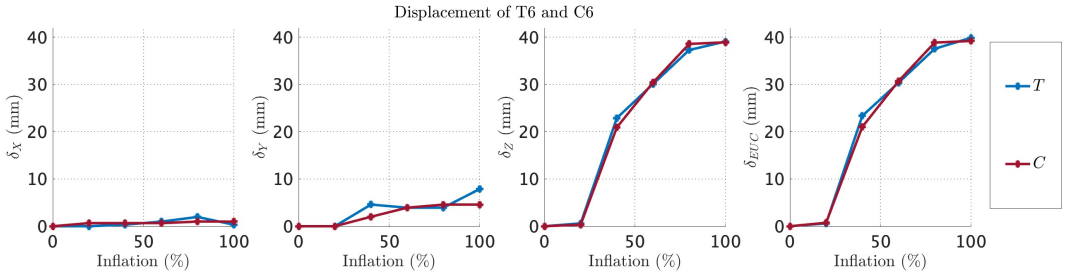

Figure A.13: *The displacement of T6 and its catheter. Based on 1 measurement*

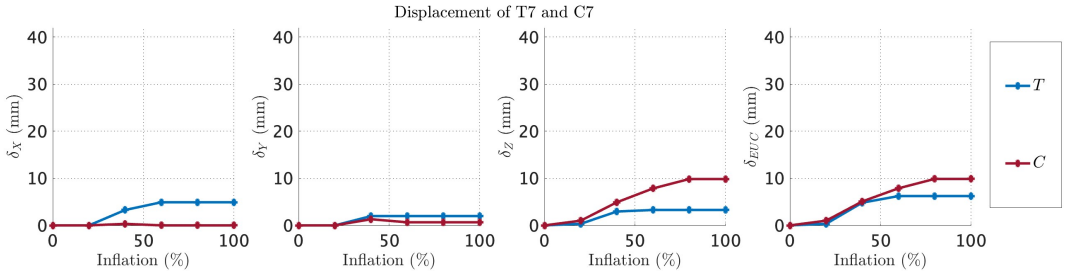

Figure A.14: *The displacement of T7 and its catheter. Based on 1 measurement*

B

Hardness scale

1. Soft tissue: the tip of the nose
2. Normal tissue: mouse on the hand (normal liver tissue)
3. Medium hard: forehead
4. Hard tissue: teeth

Based on [28] and [35].

C

Protocol

Schedule Best final test day - Nov. 16

Materials

Philips responsible

- Azurion RAMI lab
- Access to kettle for making agar
- Access to refrigerator to speed up cooling of agar
- 1 x KUKA
- 2 x needle holders for KUKA
- 8 x skin markers ClarifEye

Me responsible

- 1 x pig's liver
- 20 x bags of agar: 8 for tumor, 4 for fixation of liver (+reserve)
- 1 x Contrast medium + mini needle for aspiration
- 8 x metal fiducial (1.6 mm) (+reserve)
- 4 x Catheter with markings of lead at the end of the tip and 5 cm before it
- 1 x 13 G ablation needle
- 1 x measuring cup
- 1 x water jug
- 2 x plastic cups to make agar in
- 1 x basin in which to position the liver
- 1 x roll of tape
- 4 x Reference marker; 2 mm metal marker that serves as a reference
- 1 x bone biopsy needle (for agar and metal sphere)
- 1 x syringe for agar insertion
- 1 x permanent marker
- 1 x USB
- 1 x kitchen knife
- 1 x tea spoon
- 1 x pen
- 7 x gloves to fill with water
- 2 x gloves for myself
- 1 x air bag to simulate and inflate breathing
- 1 x Empty liver printed out on paper

Step by step approach

Make agar as surrounding tissue (5 min & 90 min waiting time)

1. Make the agar for surrounding tissue in the water jug, recipe = 4 bags with 1.5L water
2. Let cool for 1.5 hours

Prepare the bowl for use (10 min)

3. Fill 7 gloves with 100 ml water, tie them up and place them in the basin
4. Place an empty infusion bag/balloon on top of the gloves
5. Place the pig's liver on the drip bag/balloon in the basin
6. Take a picture of the setup for documentation

Place the reference markers and catheters (15 min * 4 = 60 min)

7. Create a new patient: MVD_cathrefL1
8. Grab L1-C and place in the vein as deep as possible
9. Stick L1-R on the side of the vessel with tape
10. Make a CBCT
11. Deform the liver locally so that the catheter moves
12. Make a CBCT
13. Fuse these images to check that the catheter is secure
14. Record the coordinates of L1-Ca, L1-Cb and L1-R in dView from the last CBCT
15. Try to locate them in the real liver and make black dots on the liver surface with marker to indicate the approximate location of the tumor to align with the catheter
16. Draw the Ca and Cb on the schematic liver on paper to have the location mapped out
17. End procedure
18. New patient
19. Repeat this step for L2, L3 and L4 MVD_cathrefL2, L3 and L4
20. Take a picture of the setup for documentation

Make the tumor agar markers (10 min & 5 min waiting time = 10 min)

21. Grab 2 plastic cups and turn on the kettle
22. Make the agar for 8 tumor balls, so 8 teaspoons of agar and 32 teaspoons (5 ml *32 = 160 ml) of boiling water in 1 cup
23. Keep stirring until the agar is dissolved
24. Add a small syringe (0.35*8 = 3.0) ml of contrast medium (1/20 diluted)
25. Take a picture of the setup for documentation
26. Divide it into 2 trays, put 1 already in the cooler (speeds up the cooling process), this should stand for at least 5 minutes
27. Immediately start the steps below
28. Take a picture of the setup for documentation

Inject the tumor agar markers (15 min * 4 = 60 min)

29. Create a new patient: MVD_L1-T1 (MVD_L2-T3, MVD_L3-T5, MVD_L4-T7)
30. Use ClarifEye for scheduling the agar ball
    a. Stick the skin markers on the liver
    b. Open the ClarifEye post 1 application.
    c. Click on position at top left and press the check mark 2 times

d. Click on track skin markers and click this manual
e. Make a 3D scan in thorax open CBCT
f. Find the Ca marker and select tumor 1 in line with the marker about 2cm deep in the tissue
g. Make sure the tumor is about 1cm away from the catheter marker
h. Planning > create new path, from outside toward target
i. The path to place the tumor should not be in line with the catheter (since this will be the target route)
j. Treatment > select needle and select doctors position 3
k. Now comes bullseye

31. Set up the KUKA with the bone biopsy needle for lob 1
    a. Make sure the KUKA is in T1
    b. Use the white knob on the back with X Y Z to position it
    c. If location found
    d. Move KUKA down with X (-)
    e. Lower the needle 2 cm into the tissue
32. Remove the agar from the refrigerator (the other 4 in it) and put 8ml of agar into the syringe, make sure there is no air in it
33. Screw the syringe onto the bone biopsy needle and gradually empty the syringe
34. Remove the syringe and use the biopsy needle to push the agar all the way through
35. Take a 1.6 mm metal sphere and push it into the liver with the biopsy needle
36. Pull back the KUKA X (+)
37. Repeat for MVD_L1-T2, it should be about 3 cm away from the catheter marker
38. Make a CBCT
39. Repeat for L2, L3, and L4.
40. Take a picture of the setup for documentation
41. Remove the skin markers again

Complete the setup of the liver (5 min + 15 min waiting time = 20 min)

42. Remove the surrounding agar from refrigeration
43. Pour the agar mixture around the liver so that the whole liver is fixed and make sure that about up to 1 cm of agar is thick above the liver
44. Now place the entire tub in the refrigerator for 15 minutes
45. Take a picture of the setup for documentation

Target tumors in L1 (30 min * 4 = 120 min)

46. Open patient MVD_L1-T1
47. Prepare the KUKA with 13 G ablation needle
48. Stick the skin markers from ClarifEye on the agar
49. Make a CBCT
50. Check that reference marker in CBCT field is visible
51. Schedule a needle to L1T1 as before
52. Make sure either L1-Ca or L1-Cb is in line with the puncture path.
53. Use manual bulls eye view to position the needle and position the 13 G needle
54. Insert the needle in 5 mm increments
55. Make interim CBCTs
56. Continue until you reach the L1-T1 metal marker
57. Make final CBCT

58. KUKA out
59. Repeat for same tumor from same angle
60. Repeat for MVD_L1-T2
61. Close the patient
62. Open the new patient MVD_L1-T2
63. Repeat for L2, L3 and L4.
64. Take a picture of the setup for documentation

Respiration (15 min * 2 = 30 min)

65. Open patient MVD_breath
66. Take a CBCT
67. Fill 20% of bag with air by blowing 6 times
68. Make a CBCT
69. Refill with +20%
70. Create a CBCT
71. Repeat until the bag is 100% filled
72. 100% approximately equals 500 ml
73. Repeat this cycle 1 time (more often if time to spare?).
74. Take a picture of the setup for documentation
75. Export the images to the USB

D

Workflow pictures

E ClarifEye screenshots and pictures during the experiment

Inserting catheters, checking if they are positioned correctly in the lobe.

Inserting tumor agar spheres and the markers, checking position of tumors, fixating the liver with agar

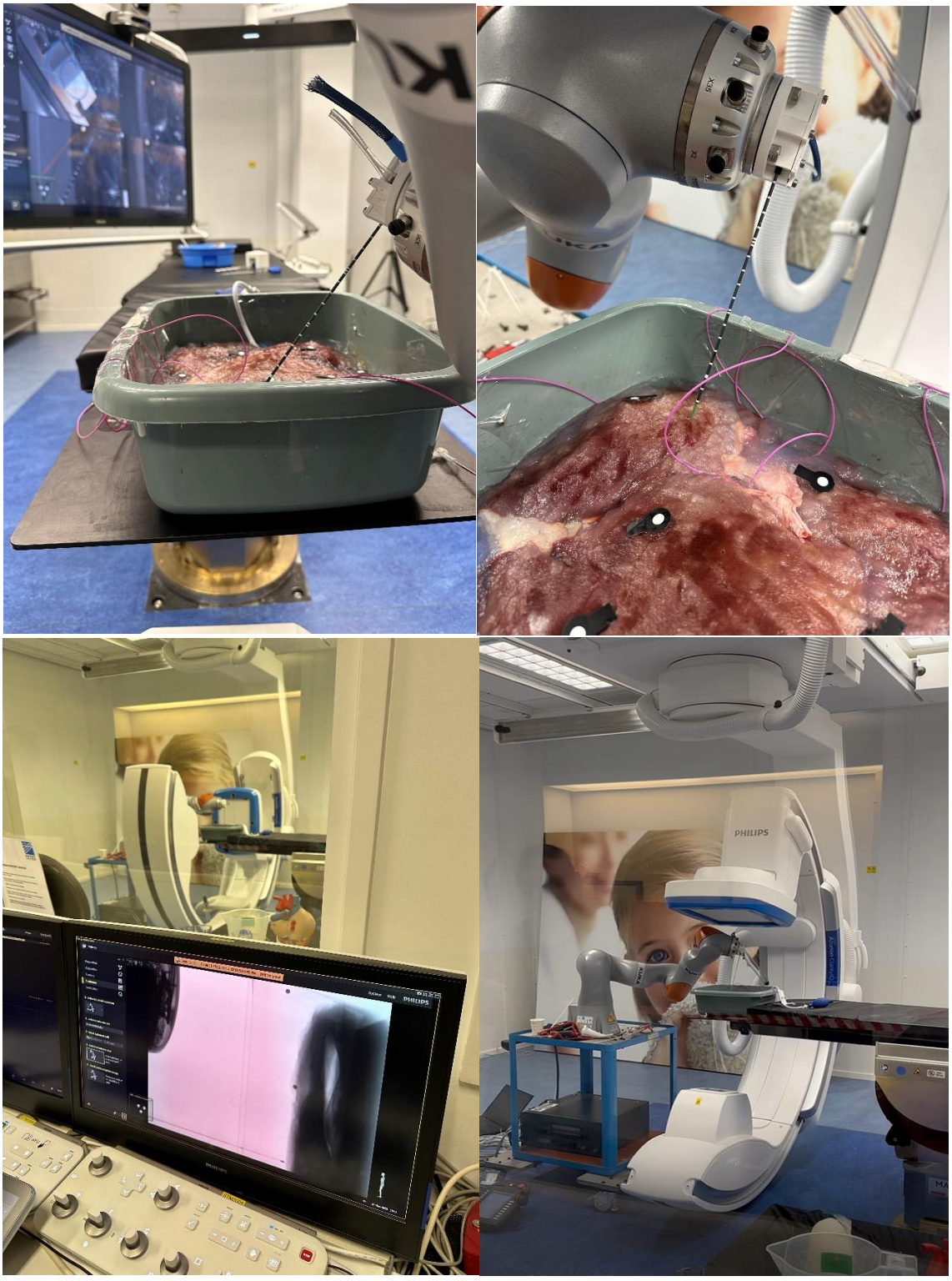

Performing needle insertions

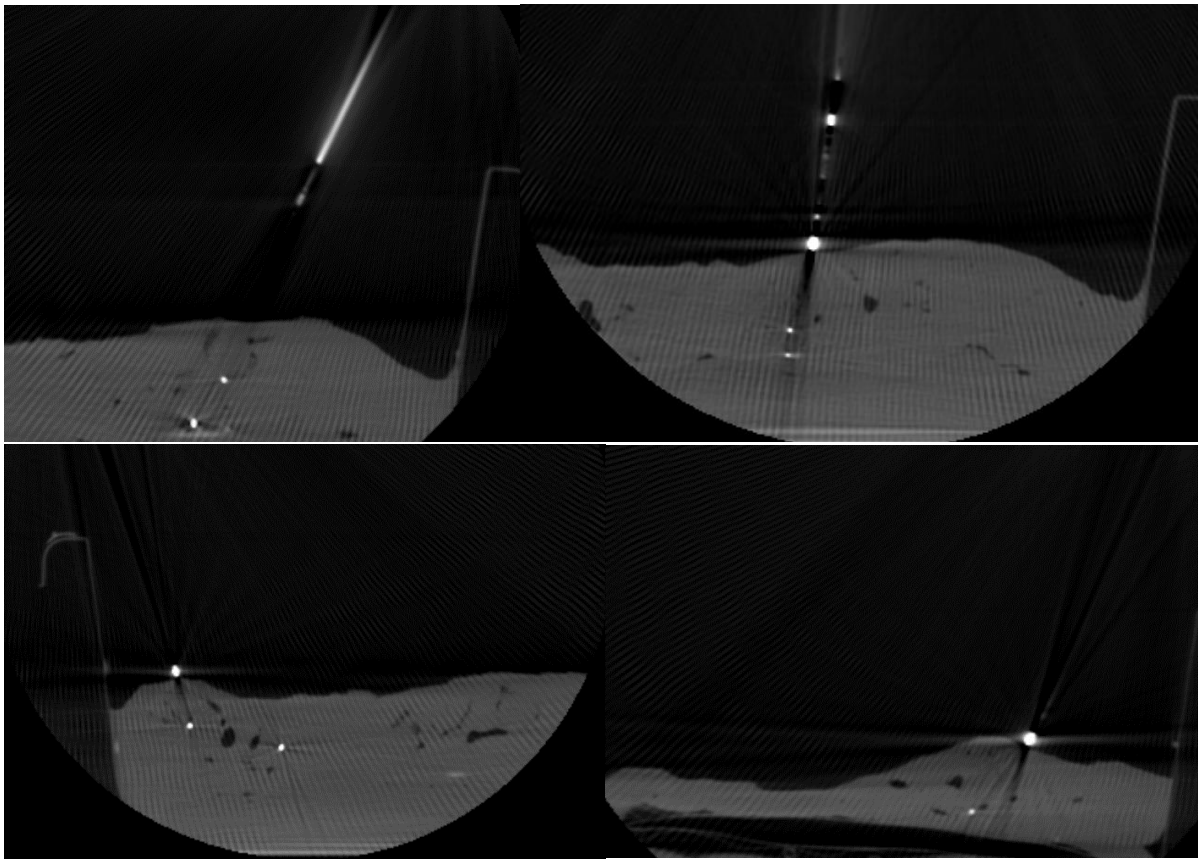

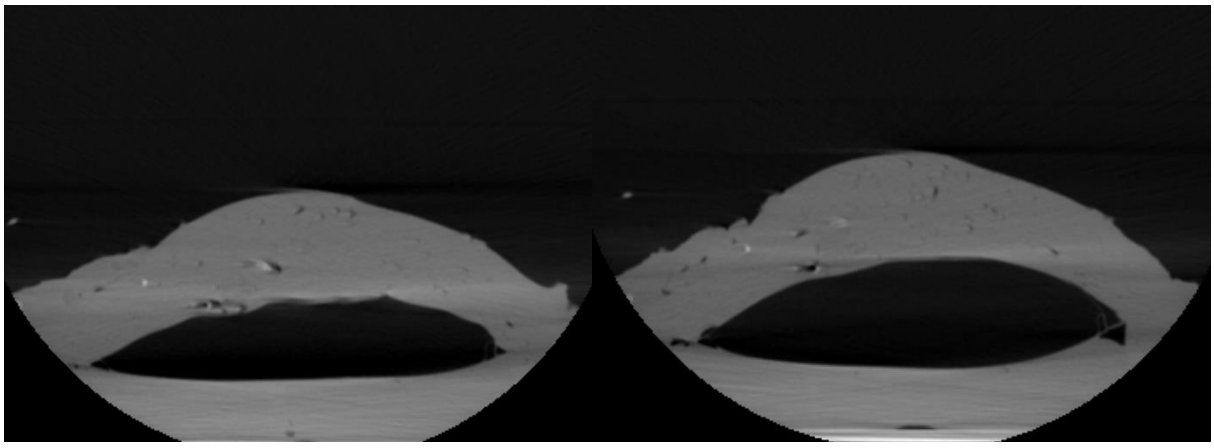

CBCT scans during needle insertion and respiratory activity

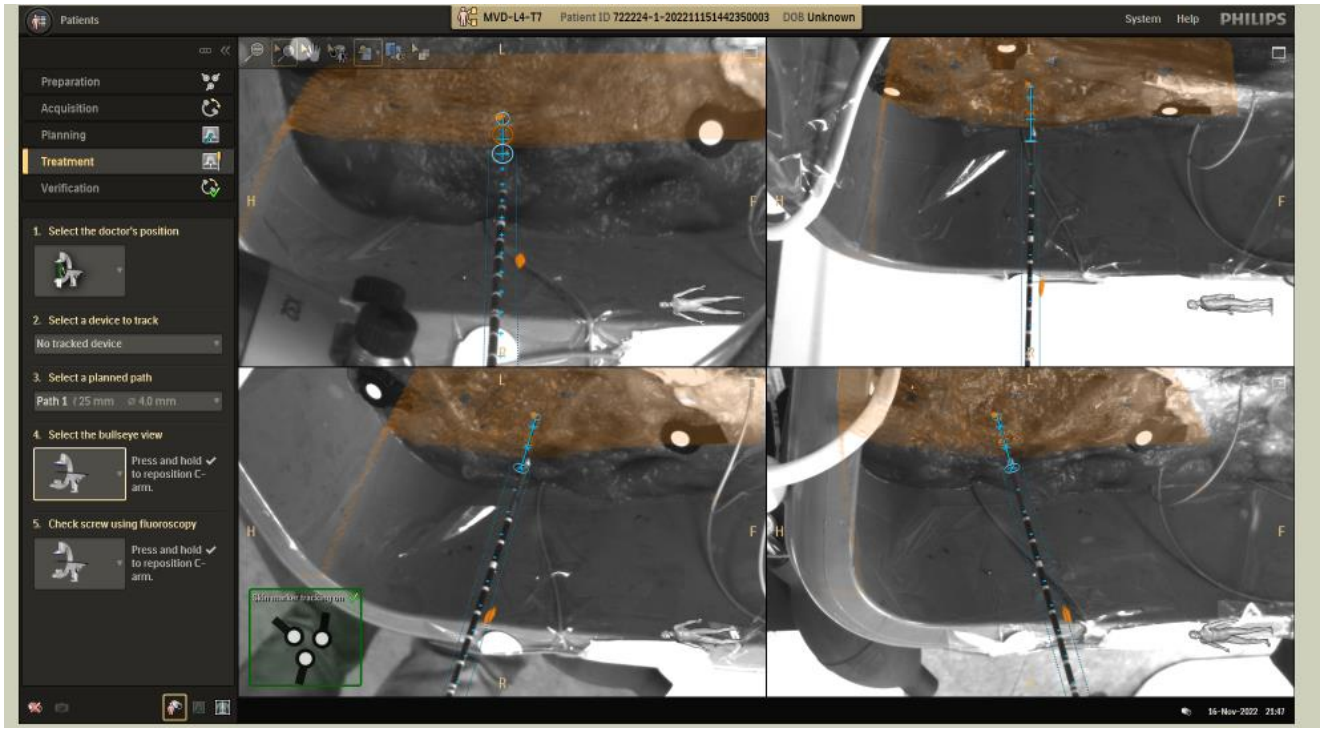

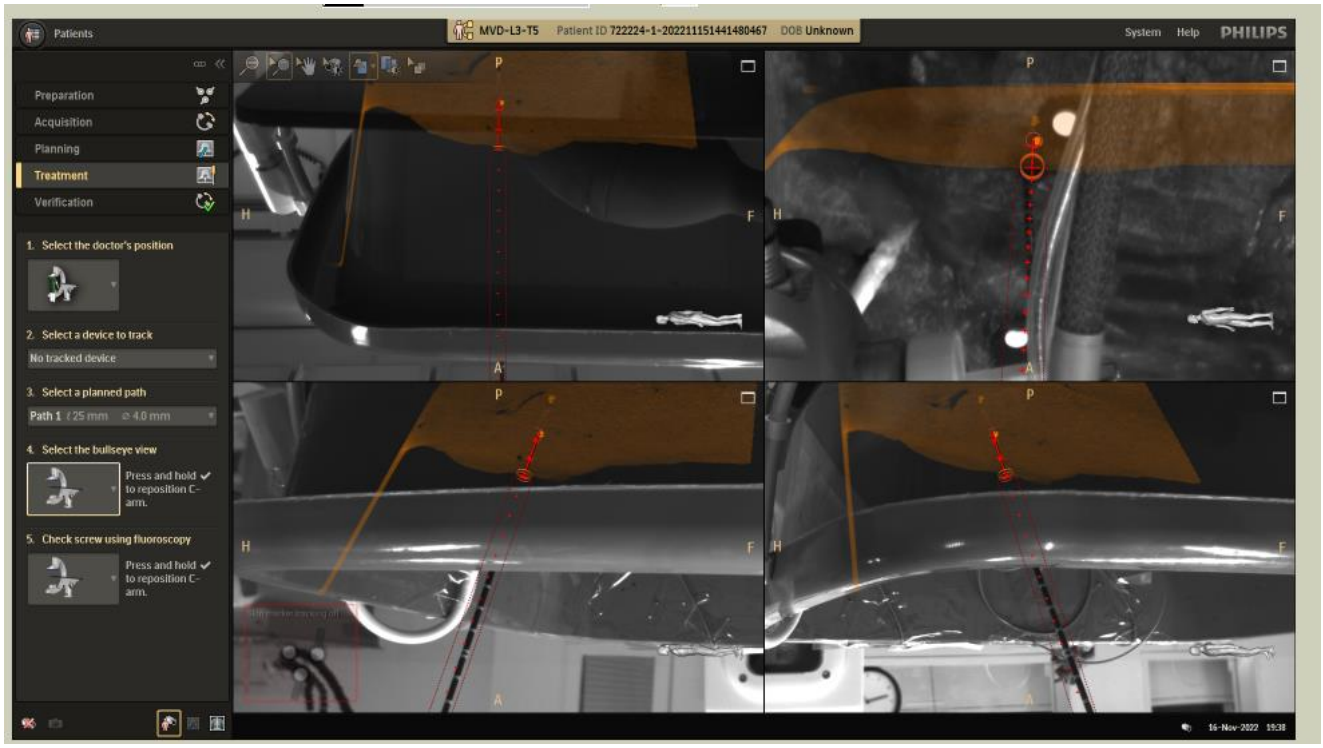

ClarifEye treatment screenshots